BACHELOR' S THESIS / BIOMEDICAL ENGINEERING 2022

Mechano-regulation study in scaffolds for tissue engineering using fluid-structure interaction models

Laia Moliner Carrillo

Universitat Pompeu Fabra Barcelona

Mechanoregulation study in scaffolds for tissue engineering using fluid-structure interaction models

Laia Moliner Carrillo

Bachelor's thesis UPF 2021/2022

Thesis supervisor(s):

Dr. Carlos Ruiz Wills and Dr. Andy L. Olivares

BCN MedTech research unit

Departament de Tecnologies de la Informació i les Comunicacions (DTIC)

Universitat Pompeu Fabra Barcelona

“To my father Sergio and my grandfather Manel, thanks for everything.
I hope you will be proud of this work.”

Acknowledgments

First of all, I want to take this opportunity to express my most sincere gratitude to my two bachelor's thesis supervisors, Professor Carlos Ruiz Wills, PhD., and Professor Andy L. Olivares, PhD., for believing that I was capable of getting through this project. It is impossible to thank you enough for your constant support and guidance and for transmitting your expertise and knowledge during the process. It was a pleasure to be helped by professionals with so much passion and dedication for their field. All your guidance, implication and patience have made this work possible.

Second, I want to thank all the BCN Medtech group members for helping me improve my work with their advice and knowledge.

I would like to acknowledge my reviewers in advance, Dr Albert Espona and pre-doc Xabier Morales, for agreeing to read my thesis; thank you for your time and support.

I am also grateful to my friends who helped me during this process. Having your company and support during this project and the entire degree was priceless. I am very honoured to share my life with people so kind and loyal.

Finally, I would like to mention all the love and encouragement I received from my family; without them, this would not be possible. I want to mention my mother, my major supporter and role model. Without her, I would not be able to be where I am today.

Abstract

The body cannot heal bone fractures surpassing 2 cm, so nowadays, graft surgery is the only available treatment. Nonetheless, this entails serious risks such as immune rejection, second medical interventions, and cross-infection. Therefore, bone tissue engineering has arisen as an alternative approach able to solve this problem. Bone tissue engineering provides temporary mechanical support for bone regeneration through an artificially prepared extracellular matrix (i.e. scaffolds) to allow cell differentiation, proliferation, and migration. To do so, global mechanical load (fluid or structural) is transferred as stimuli to cells through the scaffold architecture. Adequate mechanical characteristics, biomaterials and stimuli promote a proper mesenchymal cell differentiation to bone phenotype.

The present study aims to develop an in-silico study of bone tissue differentiation in diverse scaffold designs using fluid-structure interaction models. The relation between scaffold strain deformation and fluid mechanical stimuli developed at the cell microscopic level are analysed. The optimal configuration that leads to cell differentiation in order to restore a bone lesion is chosen. To accomplish this, on the one hand, computational solid mechanics and computational fluid transient states models were implemented for all the scaffolds with steady-state and transient state inputs. On the other hand, fluid-structure interaction models were performed considering four scenarios. Finally, cell differentiation studies considering the octahedral shear strain and fluid shear stress have been compared.

It has been found that high porous scaffolds with low transient state compression and velocity resulted in an increment in bone tissue phenotype. Moreover, it has been established that computational models not presenting interaction between solid and fluid phases can lead to overestimating bone tissue differentiation. For this reason, it is concluded that fluid-structure models are capable of mimicking and evaluating both transient state mechanical stimulations closest to reality.

Keywords

Bone tissue engineering, bone tissue differentiation, fluid-structure interaction, computational fluid transient states, computational solid mechanics, shear strain, fluid shear stress.

Preface

Medicine is constantly evolving, and one of the most promising fields is tissue engineering. Being able to repair, regenerate or even replace tissues or organs is a challenging and motivating goal. In the specific case of bone tissue engineering, the objective remains on how to be able to treat bone fractures that are wide enough to prevent self-healing.

To avoid certain risks presented in the current treatment used for these fractures, bone tissue engineering presents an alternative approach in which temporary artificial support known as a scaffold with stem cells allows the tissue healing. Nevertheless, the correct differentiation of stem cells into bone cells is crucial, which will directly depend on the scaffold properties. Due to the difficulties of studying this differentiation process in vivo, computational approaches are used to analyse the scaffold candidates. However, neither the optimal scaffold conformation nor the more realistic way to implement and evaluate the behaviour of the scaffold is already established.

Thereby, this thesis aims to design and evaluate multiple scaffold conformations with diverse geometric characteristics. To achieve this goal, three different computational approaches have been implemented, and the respective cell differentiation studies have been performed and compared. This work proposes an in-silico evaluation for the scaffold analysis performance in bone tissue engineering.

Index

1. Introduction 1
1.1 Problem and motivation 1
1.2 Objectives of the study 1
2. State of the art 2
2.1. Bone fracture 2
2.1.1. Bone healing 2
2.1.2 Current therapies 2
2.2. Bone tissue engineering 3
2.2.1. Scaffold geometries 4
2.2.2. Scaffold materials 4
2.2.3. Adaptive manufacturing approaches in BTE 4
2.2.4. Stem cells in BTE 4
2.2.5. Bioreactor in BTE 4
3.1. Cell differentiation challenge in BTE 5
3.1.1. Mechano-regulation theory in BTE 5
3.1.2. Computational approaches in BTE 5
3.1.3. Previous studies 6
3. Methodology 7
3.1. Scaffold design 8
3.2. Three-dimensional meshing 8
3.3. Mechanical characterization 9
3.3.1. Boundary conditions and displacement profiles of solid mechanics transient states model 9
3.4. Fluid characterization 10
3.4.1. Boundary conditions of computational fluid transient states model and fluid profiles 11
3.5.1. Boundary conditions of fluid-structure models and displacement/fluid profiles 12
..... 14
4. Results 14
4.1. Mechanical properties of the scaffolds 14
4.2. Cell differentiation study using Computational Solid Mechanic models 15
4.3. Cell differentiation study using Computational Fluid Transient state models 17
4.4. Cell differentiation study using Computational Solid Mechanics and Computational Fluid Transient states 20

4.5. Cell differentiation study using Fluid-Structure Interaction models..... 22
5. Discussion..... 26
6. Conclusions 28
7. Future work..... 29
References 30
Supporting information..... 33

List of figures

Figure 1. Bone healing stages: first the hematoma is formed after the fracture, second an internal callus is composed of fibrous tissue and cartilage, third a bony callus composed this time for spongy bone is created, and finally the bone remodels the callus healing the fracture completely. [18] 2
Figure 2. Bone fracture management can be divided in nonoperative techniques (left) for mild cases and operative techniques (right) for sever ones. This last option comprehends internal fixations for fractures smaller than 2 cm, and graft surgery for fractures wider than this range 3
Figure 3. Simplified scheme explaining BTE steps: assuming that it is already known the fracture location, the scaffold design is straightforward performed. Next, the scaffold is printed, the cell seeding of the patient's cells is done, and the scaffold is cultivated in a bioreactor. Finally, the scaffold is implanted on the patient's fracture gap. 3
Figure 4. Bioreactors schemes used in BTE: A) Schematic view of a spinner flask bioreactor. The scaffold contructs are attached to a needle, and shear stress is applied by convection of medium. (Extracted from [32]). B) Bioreactors systems, which nurture the development of bone tissue by supporting efficient nutrition of cultered cells and applying mechanical stimuli that are critical for functional regeneration. (Extracted from [33]). .. 5
Figure 5. Mechano-regulation concept regulating cell differentiation to mesenchymal cells form to fibrous connective tissue, fibrocartilage or bone. Two mechanical stimuli used are tissue strain and interstitial fluid flow. Curves indicate possible changes in biophysical stimuli [36] 6
Figure 6. Methodology pipeline followed during the study: (a) the six scaffolds conformations were designed, (b) the three-dimensional tetrahedral mesh was generated for the solid and fluid phase, (c) three computational approaches were performed in order to study the cell differentiation and the mechanical properties of each scaffold. 7
Figure 7. CAD diagrams of the scaffolds. Left First row: Basic cylinder porous units with 80, 70 and 60% of porosity. Second row: Basic sphere porous units with 80, 70 and 60% of porosity. Right: 60% Cylinder porous scaffold and 60% sphere porous scaffold. 8
Figure 8. Pipeline of the meshing process. First, the 3D mesh of the solid was generated using Abaqus (1). Then, the external cube was created and aligned via Meshmixer (2). Next, the 3D connective mesh of the solid and the fluid was formed (3). In the end, an error analysis of the mesh and a node connectivity evaluation were made (4). 9
Figure 9. Boundary conditions displacement profiles for CSM models. (a) For these models it was established that the bottom of the scaffold was fixed, and the top part was displaced uniformly along the Y-axis. (b) Two displacement profiles were implemented: one static (red) and the other dynamic (blue). 10
Figure 10. Boundary conditions displacement profiles for CFD models. (a) For these models was established an inlet fluid profile homogeneously applied along the Y-axis (green), a zero pressure was assumed at the outlet surface (red)., a non-slip wall boundary condition was applied to the exterior fluid walls (blue) and the interior fluid walls in contact with the scaffold (orange). b) Two fluid profiles were implemented: one as a steady state (red) and the other as transient state (blue) 11
Figure 11. Boundary conditions implemented for FSI models: (a) Models without compression; outlet was defined a zero pressure and the external nodes were not included (red), the fluid profile was homogenous applied along the Y-axis (red), a non-slip condition was applied to the exterior walls (blue), the inferior part was fixed (violet) and the information between the solid and fluid phase was done via the interaction surface

(orange). (b) Models with compression: outlet was defined a zero pressure and the external nodes were not included (red), the fluid profile was homogenous applied along the Y-axis (red), a non-slip condition was applied to the exterior walls (blue), the inferior part was fixed (violet), the superior part was displaced uniformly along the Y-axis (yellow), and the information between the solid and fluid phase was done via the interaction surface (orange). 12
Figure 12. Diagram associating bone, cartilage, or fibrous tissue differentiation on function of inlet parameters determined by the scaffold, SS and FSS [11]. 13
Figure 13. Diagram explaining the different computational approaches used in the study to determine the bone differentiation of the different scaffold conformations. (1) CSM was considered a partial study since SS results are considered but the fluid phase stimulation is excluded. (2) CFD was considered a partial study since FSS results are considered but the solid phase stimulation is excluded. (3) The correlation between the CSM and CFD results is considered a more complete study than the others previous mentioned as the solid and the fluid phase are considered but is not realistic since there is no real interaction between the fluid and the scaffold surfaces. (4) The most realistic study done in this thesis is the FSI model in which the solid and fluid phases are considered and there is interaction between the surfaces. 14
Figure 14. Elements classification depending on the type of stress subjected: (a) Compression and tension elements ratio for 60% porosity and (b) Compression and tension elements ratio for 80% porosity. 15
Figure 15. View of the 60% porosity scaffolds showing the absolute Stress and Strain scale, highlighting the compression areas in blue and black and the tension areas in red: (a) C_60 scaffold, (b) S_60 scaffold. 15
Figure 16. Cell differentiation relative to SS results in the superficial nodes using CSM at steady state compression, being bone differentiation orange, cartilage differentiation cartílage light blue and fribrous tissue differentiaion dark blue.(a) C_60, (b) S_60, (c) C_80 and (d) S_80. 16
Figure 17. Cell differentiation relative to SS results in the superficial nodes using CSM at dynamic compression, being bone differentiation orange, cartilage differentiation cartílage light blue and fribrous tissue differentiaion dark blue. (a) C_60, (b) S_60, (c) C_70 and (d) S_70, (e) C_80 and (f) S_60. 17
Figure 18. Cell differentiation relative to FSS results in the superficial nodes using CFD at steady state inlet fluid, being bone differentiation orange, cartilage differentiation cartílage light blue, fribrous tissue differentiaion dark blue and stimuli too high to promote tissue differentiation .(a) C_60, (b) S_60, (c) C_80 and (d) S_80. 18
Figure 19. Cell differentiation relative to SS results in the superficial nodes using CFD at transient state fluid profile, being bone differentiation orange, cartilage differentiation cartílage light blue and fribrous tissue differentiaion dark blue. (a) C_60, (b) S_60, (c) C_70 and (d) S_70, (e) C_80 and (f) S_60. 19
Figure 20. CFD velocity vector colour map results at maximum fluid perfusion equal to 1 mm/s (top) fluid flows that collide and then impact in the wall scaffold in C_70, (left) velocity results for C_60, and (right) velocity results for C_70. 20
Figure 21. Cell differentiation relative to S stimuli calculated with Equation 3, using the FSS results obtained with CFD models at transient state fluid perfusion and SS results obtained with CSM models at dynamic compression. Rescaled axis and presenting bone differentiation orange, cartilage differentiation cartílage light blue and fibrous tissue differentiation dark blue. (a) C_60, (b) S_60, (c) C_70 and (d) S_70, (e) C_80 and (f) C_80. 21

Figure 22. High stimuli obtained after calculating S stimuli using FSS obtained performing CFD and SS obtained performing CSM simulation. C_80 scaffold is presented in Black and S_80 scaffold in grey. 22
Figure 23. Cell differentiation relative to FSS results in the superficial nodes using FSI at dynamic transient state fluid profile with no compression, being bone differentiation orange, cartilage differentiation cartílage light blue and fibrous tissue differentiation dark blue. (a) C_60, (b) S_60, (c) C_70 and (d) S_70, (e) C_80 and (f) C_80..... 23
Figure 24. Bone differentiation comparison between FSS results obtained using FSI model with transient state fluid and no compression (black), and FSS results obtained using CFD models (grey). (a) C_60, (b) S_60, (c) C_70 and (d) S_70, (e) C_80 and (f) C_80. 24
Figure 25. SS colour map of the S_80 scaffold caused by the fluid stimuli: (left) before the fluid was perfused and () after the fluid was perfused. 25
Figure 26. Results obtained implementing a FSI model with S_80 scaffold. (a) steady state fluid and static compression and (b) with transient state fluid and dynamic compression. 25
Figure 27. SS colour map of the S_80 scaffold caused by steady state fluid perfusion at 1 mm/s and static compression of 5%: (a) before the simulation was done and (a) after the simulation was implemented. 25
Figure SI-28. Scaffolds are designed with three different porosity (60, 70 and 80%) and two geometrical pore configuration, cylindrical and spherical. 33
Figure SI-29. Elements classification depending on the type of stress subjected; Compression and tension elements ratio for 70% porosity. 33
Figure SI-30. Cell differentiation relative to SS results in the superficial nodes using CSM at steady state compression, being bone differentiation orange, cartilage differentiation cartilage light blue and fibrous tissue differentiation dark blue. (a) C_70 and (b) S_70. 34
Figure SI-31. Cell differentiation relative to FSS results in the superficial nodes using CFD at steady state inlet fluid, being bone differentiation orange, cartilage differentiation cartílage light blue, fibrous tissue differentiation dark blue, and stimuli too high to promote tissue differentiation .(a) C_70 and (b)S_70..... 34

List of tables

Table 1. Models' summary showing all the models performed in this study with their input characteristics and the scaffold in which were implemented. 7
Table 2. Properties of the six scaffolds denotated as type of porous followed by low bar and degree of porosity. For example, the cylinder porous scaffold with a porosity of 60% is named C_60. 8
Table 3. PDLLA density [26], Young's modulus [39] and Poisson's ratio [40]..... 9
Table 4. DMEM characteristics including viscosity and density [11]..... 10
Table 5. Effective Young's Modulus of each scaffold design computed with the results obtained from CSM at static compression and implementing Equation 1..... 14

1. Introduction

1.1 Problem and motivation

It is estimated that, in 2019, there were 178 million new fractures, most of them as a result of a trauma (car accident, sports injury, among others) [1, 2]. The risk of a fracture increases with age, and it is greatest in women [3]. Therefore, the worldwide incidence of bone fractures has risen steeply in the latest years, increasing in Europe at an annual rate of 28% [4].

Although it is widely known that the body is capable of self-healing, there are some lesions that the body is not able to restore by its own mechanisms. In the specific case of bone tissue, when the bone defect area exceeds the range of 2cm, it cannot be repaired or restored [5]. Consequently, bone transplantation has become an effective treatment, but bone graft surgery is restricted to the limitations of autologous and allogeneic bones (insufficient bone source, immune rejection, secondary surgery, cross-infection, and so on) [6]. Therefore, bone tissue engineering (BTE) has arisen as an alternative approach able to solve this problem.

BTE aims to introduce new functional bone regeneration via the cooperative combination of biomaterials, stem cells, and factor therapy [7]. To accomplish this objective, the artificially prepared temporary extracellular matrix, also known as a scaffold, is required to allow cell differentiation, proliferation, and migration [5,8].

Nevertheless, there are existing challenges that prevent the clinical application of BTE. One of the biggest problems that must be overcome, is the stem cells' differentiation into osteogenic lineage during all the procedures [9]. This cornerstone is directly linked with the mechanical stimuli received by the cell through the scaffold. Therefore, it is essential to understand how an artificial designed ECM could transmit fluid flow stresses and mechanical deformations to its surfaces. Employing in vivo analysis to study this can be complex and costly, for these reasons computational approaches have been used in recent years [10].

Computational fluid transient states have been broadly applied to link scaffold configuration to fluid shear stress (FSS) behaviour in BTE [11, 12, 13]. In addition, recent studies have introduced the use of Fluid-Structure Interaction (FSI) models to study the impact that mechanical compression could affect FSS results [14, 15]. However, these studies are only considering the FSS outcome to evaluate the scaffold viability, without also analysing the direct impact that shear strain (SS) has in the cell differentiation. For this reason, there is a need for studies capable of mimicking and evaluating both transient state mechanical stimulations to mirror the closest possible to reality.

1.2 Objectives of the study

Considering the problematics mentioned above, the primary purpose of this study is to conduct a fluid-structure analysis on different scaffold structures to prove the potential power of tissue formation.

The transient state interactions between scaffold strain deformation and fluid mechanical stimuli developed at the cell microscopic level are analysed on scaffold geometries with various porosities and conformations. The study focuses on the optimal configuration that leads to cell differentiation and cell adhesion in order to restore a bone lesion.

2. State of the art

2.1. Bone fracture

Bone fracture is a full or partial break in the continuity of bone tissue and could occur in any bone in the body. It is possible to discern between closed fracture and compound fracture. The first one occurs when the bone break does not damage the surrounding tissue. Contrarily, the second one happens when there is existing damage, which leads to major risks for the patient [16].

2.1.1. Bone healing

Fracture healing is a complex process and can be influenced by the type of fracture, the patient characteristics, and treatment factors. Currently, the healing process can be separated into four different stages:1) hematoma formation; 2) fibrocartilaginous callus formation; 3) bony callus formation; 4) bone remodelling (Figure 1) [17, 18].

If the fracture gap is smaller than 0.01mm there is no need for callus formation (stages 2 and 3 of the healing process are skipped), which is called primary healing. Conversely, if the fracture gap surpasses this range, the four steps must be followed, named secondary healing [19].

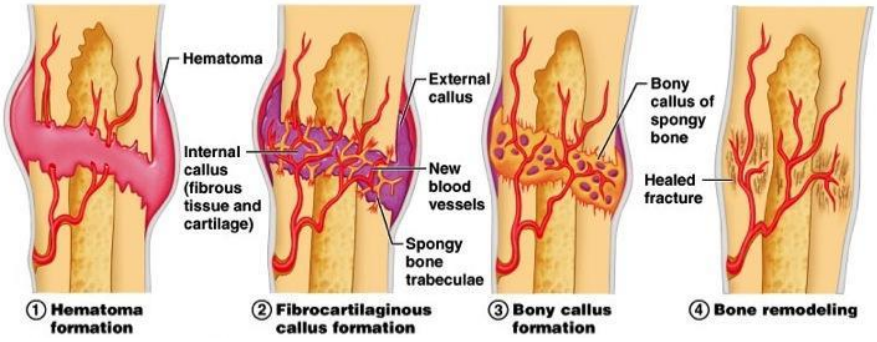

Figure 1. *Bone healing stages: first the hematoma is formed after the fracture, second an internal callus is composed of fibrous tissue and cartilage, third a bony callus composed this time for spongy bone is created, and finally the bone remodels the callus healing the fracture completely. [18]*

2.1.2. Current therapies

Fracture management can be divided into nonoperative and operative techniques (Figure 2). The nonoperative approach consists of a closed reduction if required, followed by a period of immobilisation with casting or splinting [20]. On the contrary, if the fracture cannot be healed only by performing an immobilisation, operative techniques are needed. In cases involving compound fractures (bone is visible through the skin) or joints, they require surgery in which the surgeon carries out an internal fixation using pints, plates, or screws [21].

However, when the defect bone area exceeds a defined range (*>2cm*) it cannot be repaired or restored [5]. In these situations, a surgical procedure is followed using transplanted bone to repair and rebuild the damaged bone. These types of interventions are usually due to the previous knowledge of a nonunion fracture, or the presence of a specific bone condition [22]. Although graft surgery is broadly used, there are existing limitations regarding autologous (bone from the patient) and allogeneic (from other individuals) bones (insufficient bone source, immune rejection, secondary surgery, cross-infection, and so on) [6].

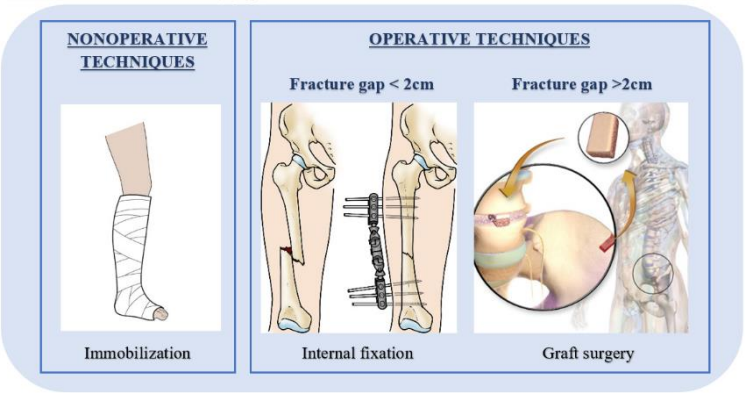

Figure 2. *Bone fracture management can be divided in nonoperative techniques (left) for mild cases and operative techniques (right) for sever ones. This last option comprehends internal fixations for fractures smaller than 2 cm, and graft surgery for fractures wider than this range*

2.2. Bone tissue engineering

BTE aims to introduce new functional bone regeneration via the cooperative combination of biomaterials, cells, and factor therapy [7]. The concept is to transplant a biofactor (cells, genes and/or proteins) within a porous degradable material known as a scaffold (Figure 3). The biofactors, which include stem-cell and gene therapy approaches, are used to stimulate tissue repair [23].

To accomplish this objective, the scaffold must facilitate cell migration and provide the necessary support for the cells to proliferate and differentiate [5,24]. Moreover, the artificial ECM should balance mechanical function with biofactor delivery, providing a sequential transition in which the regenerated tissue assumes function as the scaffold degrades [23].

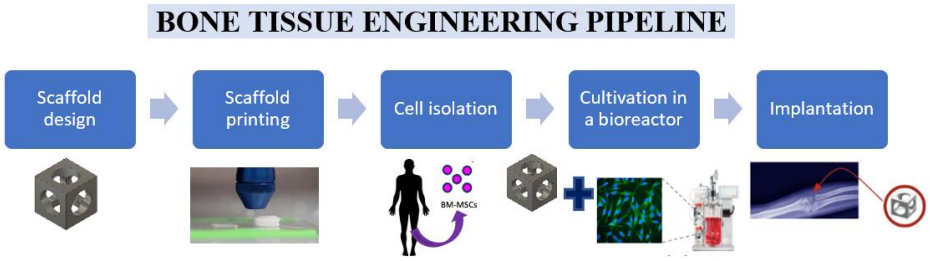

Figure 3. *Simplified scheme explaining BTE steps: assuming that it is already known the fracture location, the scaffold design is straightforward performed. Next, the scaffold is printed, the cell seeding of the patient's cells is done, and the scaffold is cultivated in a bioreactor. Finally, the scaffold is implanted on the patient's fracture gap.*

2.2.1. Scaffold geometries

Bone scaffolds must fulfil some essential structural requirements in order to provide adequate performance. First, the scaffold should be a 3D porous structure with high connectivity, supporting and maintaining the original tissue shape and providing support and channels for cell seeding, proliferation and differentiation, vascularization, and transportation of nutrients and metabolic waste. Second, the mechanical properties of the scaffolds should match the implant site to ensure mechanical stability in the healing process and avoid stress shielding (reduction of bone density due to the removal of typical stress) [5,24].

2.2.2. Scaffold materials

Bone scaffolds not only have to accomplish certain geometry demands but also materials related. Scaffolds must be biocompatible and non-toxic, as well as biologically active, and can interact with surrounding tissues or organs [5]. Additionally, the material surface chemistry should be adequate to allow cells to adhere and express their normal phenotypes, and it has to equally include a correct biodegradability after sufficient bone formation [24]. Consequently, a wide range of ceramics, polymers, and composites have been analysed as biomaterials in BTE studies. Natural biomaterials as autografts and allografts have some limitations as was mentioned before. For instance, ceramics materials based on calcium phosphates and bioglasses have good osteoinductive properties (ability to induce new bone formation) but low mechanical properties and difficulties in forming process. On the other hand, polymers such as those derived from polyglycolic acid (PGA) and polylactic acid (PLA) have easy formability, good mechanical properties, and biodegradability which may vary according to their molecular weight but low osteoinductive capacity [25, 26].

2.2.3. Adaptive manufacturing approaches in BTE

Taking into consideration the aspects mentioned before regarding geometry conformation scaffolds and biomaterials used, it is not unreasonable to think that traditional manufacturing processes are not an optimal option. Contrarily, adaptive manufacturing (AM) approaches can create scaffolds with tailored porosity for specific fractures. For instance, 3D printing (3DP), solid freeform fabrication (SFF), rapid prototyping (RP), are different AM approaches that allow complex shapes for scaffolds' fabrication directly from a Computer Aided Design (CAD) file [27].

2.2.4. Stem cells in BTE

BTE requires a reliable stem cell source, in addition to appropriate scaffolds and growth factors. Control over the differentiation of mesenchymal stem cells (MSCs) makes them attractive cell sources for BTE [28]. In fact, bone marrow derived MSCs are the most frequently employed. Moreover, it is important to consider that MSCs differentiation needs to be governed by a 3D environment as biomaterial features, mechanical stimuli, and molecular mechanisms are involved in MSC responses [29].

2.2.5. Bioreactor in BTE

A bioreactor is a vessel in which biochemical or biological processes involving cells, organisms, or biochemically active substances are carried out under closely monitored and tightly controlled operating conditions (e.g., temperature, pH, flow rate, nutrient and oxygen supply, and so on) (Figure 4.A) [30].

In the case of BTE, before the implantation into the body, the cell-containing constructs are often cultured in vitro to increase cell proliferation on the scaffold and to allow for differentiation of the stem cells into osteoblasts. Bioreactor systems are used to alleviate this nutrient transfer limitation by continuously mixing media and by convectively transporting nutrients to cells (Figure 4.B) [31].

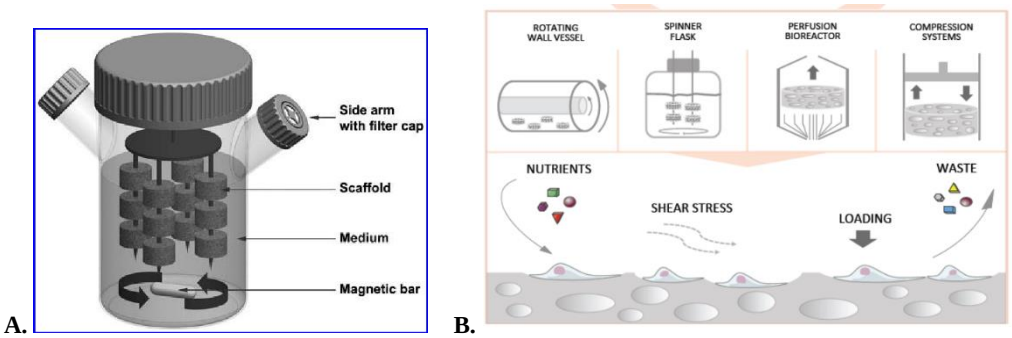

Figure 4. *Bioreactors schemes used in BTE: A) Schematic view of a spinner flask bioreactor. The scaffold contructs are attached to a needle, and shear stress is applied by convection of medium. (Extracted from [32]). B) Bioreactors systems, which nurture the development of bone tissue by supporting efficient nutrition of cultered cells and applying mechanical stimuli that are critical for functional regeneration. (Extracted from [33]).*

3.1. Cell differentiation challenge in BTE

BTE remains a challenge in the clinic, and one of the most limiting problems remains in the regulation of stem cell differentiation during all the process [9].

3.1.1. Mechano-regulation theory in BTE

This cornerstone is controlled by the mechanotransduction pathway, that can be defined as the mechanism through which cells convert mechanical stimuli into biomechanical responses. It is known that superficial mechanoreceptors of cells sense the mechanical stimulus, which are transmitted to the nucleus via the actin skeleton or chemical pathways. Then, the nucleus responds to these signals by upregulating or downregulating the expressions of certain genes [9].

Recent studies prove that BMSCs differentiation towards osteogenic lineage is regulated by external mechanical simulation. These external inputs can be caused by the micro-deformation of the perilacunar bone matrix and by the shear stresses generated due to the canaliculi fluid flow [9]. Therefore, a quantitative analysis is necessary in order to verify if the design of a scaffold meets the requirements necessary for bone tissue differentiation. Nonetheless, due to lack of experimental technology capable of correlating the mechanical SS and FSS to biomechanical responses, numerical simulation has become an effective analysis method [9, 14].

3.1.2. Computational approaches in BTE

Nowadays, there are different existing computational approaches to approach BTE, the one most commonly used is known as Computational Fluid Transient states (CFD). Which can be defined as a branch of fluid mechanics that uses computer-based numerical analysis to solve problems in fluid flow [34]. This analysis is widely used to study the FSS and fluid path, using it as a predictive tool. Since it provides significant information

about the interaction of scaffold and stresses, which is key for evaluating the scaffold characteristics and its biological viability [22, 35].

Another approach used in these recent years is Fluid-Structure Interaction, a multiphysics coupling between the laws that describe fluid transient states and structural mechanics [36]. This technique has been recently used in BTE, as it is a powerful tool to link mechanical deformation produced by the scaffold with cell biological behavior (Fig. 5). Allowing to predict the osteogenic differentiation of bone scaffold. The combination of both tools gives a more complete analysis that makes possible the correct evaluation of achievable tissue restoration [35].

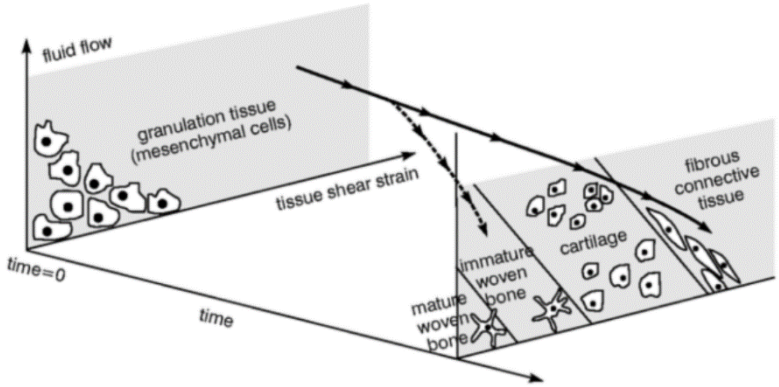

Figure 5. *Mechano-regulation concept regulating cell differentiation to mesenchymal cells form to fibrous connective tissue, fibrocartilage or bone. Two mechanical stimuli used are tissue strain and interstitial fluid flow. Curves indicate possible changes in biophysical stimuli [36].*

3.1.3. Previous studies

Several studies have been done in order to correlate scaffold characteristics to FSS outcomes. Ali et al. used CFD analysis to study the effect of surface roughness on scaffold permeability and fluid flow induced FSS and concluded that high roughness decreased FSS. Ouyang et al. studied the effect of pore size on hydro-mechanical properties and stated that flow velocity linearly increased with the pore size. Other studies have introduced the FSI approach to analyse the effect of compression stimulation on the FSS result values. Zhao et al. used CFD and FSI models to quantify the FSS of different scaffold geometries (architecture, pore size and porosity) under the combination of fluid perfusion and compression loading scenarios and concluded that the combination of both stimuli caused amplified FSS. In the case of Fu et al. study, it was also used the combination of CFD and FSI approaches to examine the permeability and FSS ranges of different scaffold configurations applying steady state mechanical inputs. Therefore, they showed that if the pore size increases the FSS will also increase.

3. Methodology

The methodology of this study is divided into different sections as shown in Figure 6: the different scaffolds conformations were designed; the 3D meshing was generated; computational solid mechanics models were implemented for all the scaffolds with steady state compression and transient state one; computational fluid transient states were performed to all the scaffolds with steady state fluid profile and transient state one; and finally, four different scenarios were evaluated using fluid-structure interaction. Furthermore, all the simulation results were analysed using MATLAB (Version). Therefore, overall, 38 simulations were performed as it is detailed in Table 1.

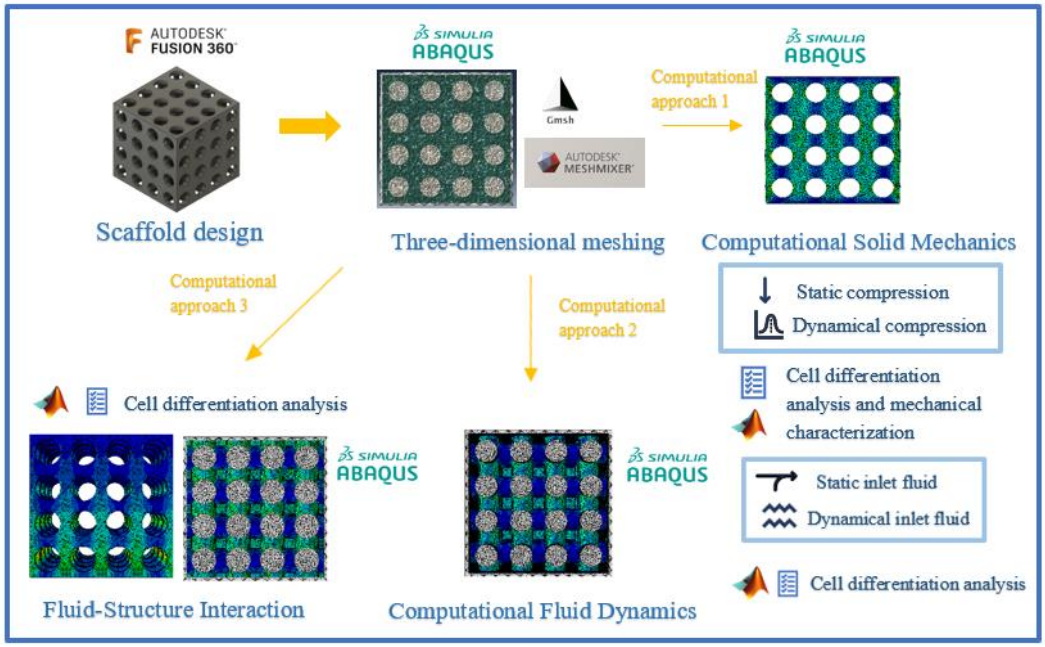

Figure 6. *Methodology pipeline followed during the study: (a) the six scaffolds conformations were designed, (b) the three-dimensional tetrahedral mesh was generated for the solid and fluid phase, (c) three computational approaches were performed in order to study the cell differentiation and the mechanical properties of each scaffold.*

Table 1. *Models' summary showing all the models performed in this study with their input characteristics and the scaffold in which were implemented.*

Scaffold/Model type	C_60	C_70	C_80	S_60	S_70	S_80
CSM: static compression	✓	✓	✓	✓	✓	✓
CSM: dynamical compression	✓	✓	✓	✓	✓	✓
CFD: static fluid profile	✓	✓	✓	✓	✓	✓
CFD: dynamic fluid profile	✓	✓	✓	✓	✓	✓
FSI: static fluid profile & no compression	✓	✓	✓	✓	✓	✓
FSI: dynamic fluid profile & no compression	✓	✓	✓	✓	✓	✓
FSI: dynamical fluid profile & static compression	✗	✗	✗	✗	✗	✓
FSI: dynamical fluid profile & dynamic compression	✗	✗	✗	✗	✗	✓

3.1. Scaffold design

In this study, two cubic regular architectures were selected following the design proposed by Fu et al.: cylinder pore based (C), and sphere pore based (S). The design size of each model was 2 x 2 x 2 mm, which was generated by the coupling of 0.5mm basic units (Fig.7 and Fig. SI-28) using the software Fusion360 (Autodesk, Inc). Three levels of porosity were contemplated: 60, 70, and 80% based on previous experimental studies [37]. In total, 9 different geometries were evaluated with disparate characteristics (Table 2).

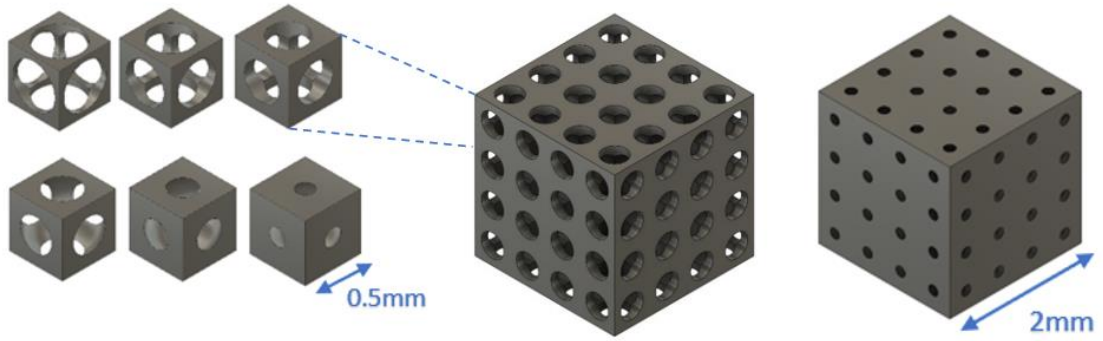

Figure 7. *CAD diagrams of the scaffolds. Left First row: Basic cylinder porous units with 80, 70 and 60% of porosity. Second row: Basic sphere porous units with 80, 70 and 60% of porosity. Right: 60% Cylinder porous scaffold and 60% sphere porous scaffold.*

Table 2. *Properties of the six scaffolds denotated as type of porous followed by low bar and degree of porosity. For example, the cylinder porous scaffold with a porosity of 60% is named C_60.*

	C_60	C_70	C_80	S_60	S_70	S_80
Porosity (%)	60	70	80	60	70	80
Porous diameter (mm)	0.32	0.36	0.41	0.143	0.229	0.294
Surface area (mm2)	57.18	52.42	43.69	70.56	64.27	57.13

3.2. Three-dimensional meshing

The steps followed to generate the 3D mesh of the scaffolds are shown in Figure 8. First, the scaffolds generated were segmented in Abaqus 2018 (Dessalut Systèmes) to create an optimal tetrahedral 3D mesh of the solid. The mesh size was established at 0.05 mm considering the computational cost, the possible error approximation, and that cell diameter oscillates around 0.01 mm [45]. Then, a fluid boundary was created with the insertion of an external cube of 2.1 mm of dimension using Meshmixer[1]. Afterward, the external cube and the scaffold were aligned. The next step was the 3D connective mesh formation of the solid and the fluid region via Gmsh[2] . Finally, nodes connectivity and error of the mesh were evaluated by Abaqus.

[1] www.meshmixer.com
[2] www.gmsh.info

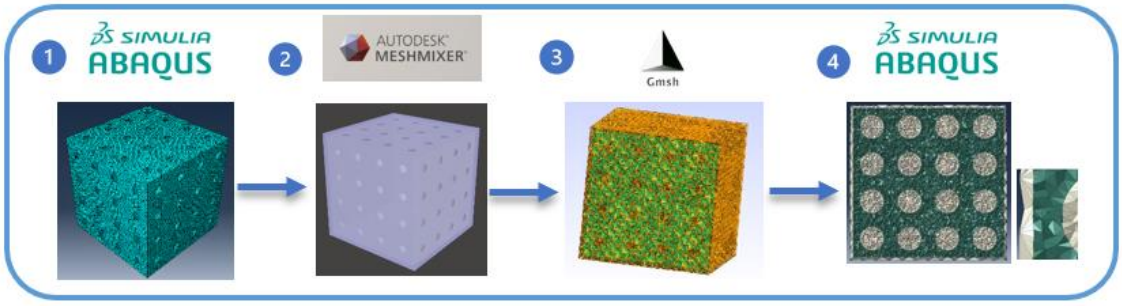

Figure 8. *Pipeline of the meshing process. First, the 3D mesh of the solid was generated using Abaqus (1). Then, the external cube was created and aligned via Meshmixer (2). Next, the 3D connective mesh of the solid and the fluid was formed (3). In the end, an error analysis of the mesh and a node connectivity evaluation were made (4).*

3.3. Mechanical characterization

In order to prove if the scaffold mechanical properties were similar to bone characteristics, a mechanical compression test was done for each scaffold using Abaqus 2018 (Dessault Systèmes). The scaffold material for all conformations was Poly-D, L-lactic acid (PDLLA) following a linear elastic behaviour, and which parameters are indicated in Table 3.

Table 3. *PDLLA density [26], Young's modulus [39] and Poisson's ratio [40].*

Material	Density (kg/m3)	Young's modulus (GPa)	Poisson's ratio
PDLLA	1260	2	0.331

3.3.1. Boundary conditions and displacement profiles of solid mechanics transient states model

The simulations were performed establishing the boundary conditions shown in Figure 9.A. The whole lower surface of the scaffold was subjected to fixed constraints and the upper surface was displaced uniformly along the Y-axis at a speed equal to1 mm/min. The maximum compression achieved in the simulations was equal to 5% displacement relative to the height of the scaffold, meaning a total of 0.1 mm. Therefore, the models were evaluated with two different displacement profiles: steady state compression and transient state compression (Fig.9.B). The first type was performed, stipulating an unchanging displacement of 0.1 mm in the negative Y-axis for 0.1 seconds, equivalent to a 5% compression. The second type of displacement was performed completing a cycle that lasted 0.2 seconds as can be seen in Figure 9.B.

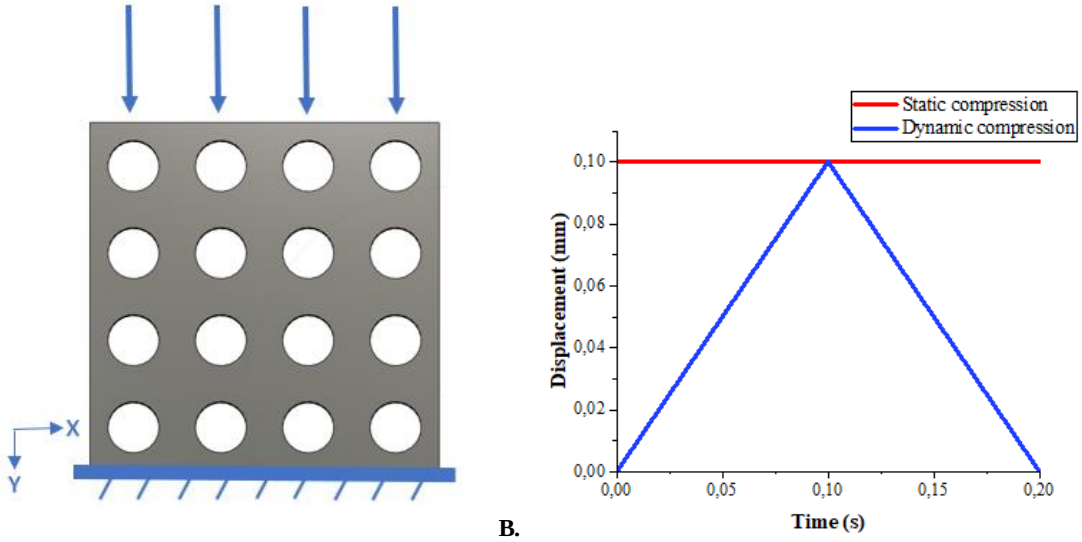

A. **B.**

Figure 9. *Boundary conditions displacement profiles for CSM models. (a) For these models it was established that the bottom of the scaffold was fixed, and the top part was displaced uniformly along the Y-axis. (b) Two displacement profiles were implemented: one static (red) and the other dynamic (blue).*

The shear strain components and the reaction force were extracted from the simulation. Then, the Effective Young's Modulus (E) was calculated using Equation 1 and the SS was computed using Equation 2.

$$E_f = (R/A)/(\Delta l/l) \quad (1)$$

Equation 1. *Effective Young's Modulus formula calculated via the reaction force (R), the cross-section area of the scaffold (A) and the axial strain* (Δl/l). *[11]*

$$SS = \frac{2}{3}\sqrt{(\varepsilon_1 - \varepsilon_2)^2 + (\varepsilon_2 - \varepsilon_3)^2 + (\varepsilon_3 - \varepsilon_1)^2} \quad (2)$$

Equation 2. *Octahedral shear strain formula using the shear strain components (maximum, medium and minimum). [11]*

3.4. Fluid characterization

Computational fluid transient state models were computed using Abaqus 2018 (Dessault Systèmes) following Navier-Stokes equations. The fluid was a cell culture media known as Dulbecco's modified Eagle medium (DMEM) modelled as Newtonian fluid with the transient state viscosity and density indicated in Table 4, and assuming a laminar flow.

Table 4. *DMEM characteristics including viscosity and density [11].*

Material	Viscosity (Pa·s)	Density (Kg/m3)
DMEM	$1.45 \cdot 10^{-3}$	1000

3.4.1. Boundary conditions of computational fluid transient states model and fluid profiles

Some boundary conditions were defined as it can be seen in Figure 10.A. An inlet fluid profile was homogenous applied along the Y-axis at 1 mm/s, and a zero pressure was assumed at the outlet [11,12]. A non-slip wall boundary condition was applied to the exterior fluid walls and the interior fluid walls in contact with the scaffold. Furthermore, a predefined field with a velocity of 0 at the initial step was also implemented.

Moreover, two fluid profiles were tested to examine the different responses to the stimulus. On the one hand, for the steady state fluid profile, a constant fluid velocity equal to 1 mm/s for 0.1 seconds was established (Fig. 10.B). On the other hand, the transient state fluid profile was stipulated following a cycle of 0.2 seconds as can be seen in Figure 10.B.

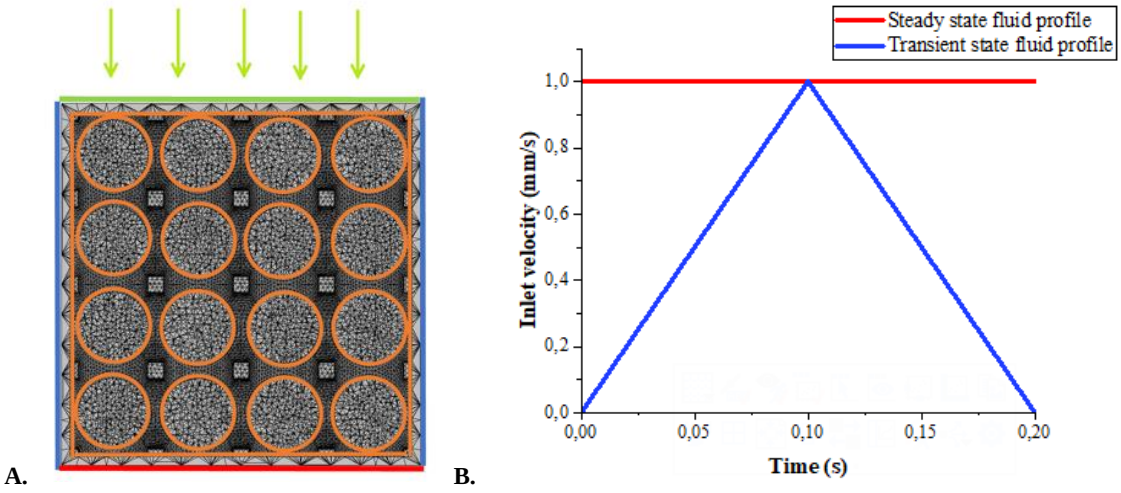

Figure 10. *Boundary conditions displacement profiles for CFD models. (a) For these models was established an inlet fluid profile homogeneously applied along the Y-axis (green), a zero pressure was assumed at the outlet surface (red)., a non-slip wall boundary condition was applied to the exterior fluid walls (blue) and the interior fluid walls in contact with the scaffold (orange). b) Two fluid profiles were implemented: one as a steady state (red) and the other as transient state (blue).*

3.5. Fluid-Structure interaction

After simulating the solid and the fluid phases separately, the real time interactions between the scaffold and the fluid were evaluated through fluid-structure interaction models. Therefore, to be as accurate as possible to reality, the models were based on a specific bioreactor design. Within this bioreactor the fluid could freely transport through the scaffold ends under mechanical displacement, and the scaffold is laterally confined. Furthermore, four cases were studied: a) static fluid profile without compression, b) dynamic fluid profile without compression, c) dynamic fluid profile with static compression, and d) dynamical fluid profile with dynamical compression. The strain components, FSS, fluid velocity and fluid pressure were computed using Abaqus 2018 (Dessault Systèmes). Besides SS was calculated using Equation 2.

3.5.1. Boundary conditions of fluid-structure models and displacement/fluid profiles

As previously mentioned, the models follow a particular bioreactor design, hence the boundary conditions were as can be seen in Figure 11. For the fluid model: the outlet was defined a zero pressure; the particular fluid profile was homogenous applied along the Y-axis; and a non-slip condition was applied to the exterior walls. For the solid model: the inferior part was fixed; and the superior part was displaced uniformly along the Y-axis with a steady or transient state compression profile. Moreover, both models were connected for the interaction surface, that scaffold was defined as the interior fluid wall and the exterior scaffold wall. However, the top and bottom surfaces have to be excluded from the interaction surface since there were certain restrictions and displacement already implemented.

As was anterior specified, four cases had been studied considering the interaction between the solid and the fluid. Nevertheless, the last cases involving compression stimulus were only evaluated for one sphere pore-based scaffold. The selection was done after analysing the performance of the different scaffolds for the FSI models without compression. Therefore, the scaffold that obtained better results, was selected to be evaluated with compression.

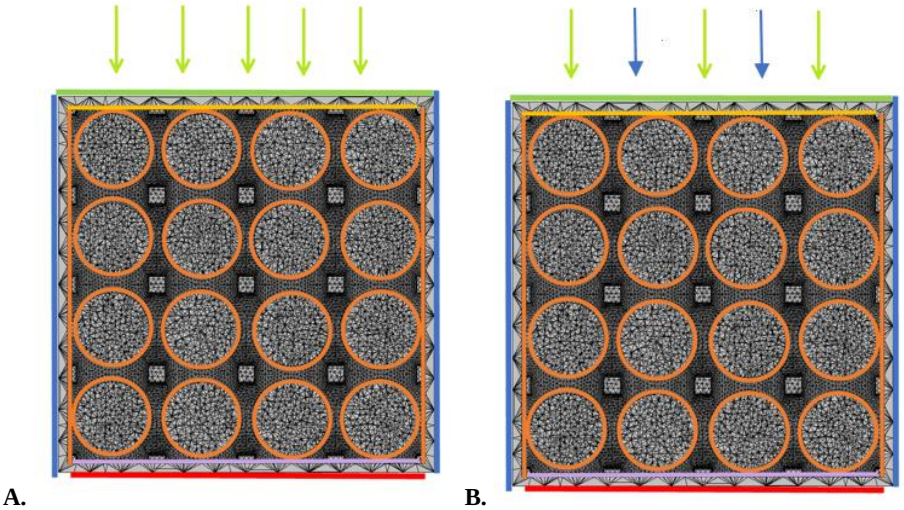

A. **B.**

Figure 11. *Boundary conditions implemented for FSI models: (a) Models without compression; outlet was defined a zero pressure and the external nodes were not included (red), the fluid profile was homogenous applied along the Y-axis (red), a non-slip condition was applied to the exterior walls (blue), the inferior part was fixed (violet) and the information between the solid and fluid phase was done via the interaction surface (orange). (b) Models with compression: outlet was defined a zero pressure and the external nodes were not included (red), the fluid profile was homogenous applied along the Y-axis (red), a non-slip condition was applied to the exterior walls (blue), the inferior part was fixed (violet), the superior part was displaced uniformly along the Y-axis (yellow), and the information between the solid and fluid phase was done via the interaction surface (orange).*

3.6. Cell differentiation study

For the purpose of evaluating the cell differentiation occurring in the scaffold surfaces the figure proposed by Olivares et al. 2009 was implemented (Fig. 12). This diagram describes the scaffold surface percentage associated with bone, cartilage, or fibrous tissue on function of the inlet parameters. To do so, the mechano-regulation theory proposed by Prendergast et al. 1997 was modified to include the SS from the solid phase and the fluid shear stress from the liquid phase. Consequently, the SS and FSS obtained from the

simulations had been used to compute the stimuli S on the wall of the scaffold using Eq. 3. If 10^{-2} > S, the stimuli is too low to induce any type of tissue phenotype, and if S>6 the stimuli will be too high to induce differentiation. If 3>S>1, then the cartilage tissue differentiation occurs, 6>S>3, then fibrous tissue differentiation occurs, and if 1>S>10^{-2} bone differentiation occurs [11,35,41].

$$S = \frac{SS}{a} + \frac{FSS}{b} \tag{3}$$

Equation 3. *Stimuli S computed using the octahedral shear strain (SS) and the fluid shear stress (FSS). Where a is equal to 0.0375% and b is equal to 10mPa. [11]*

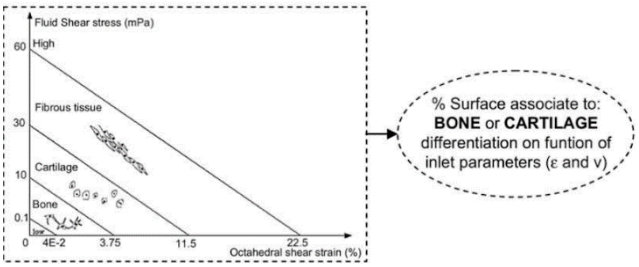

Figure 12. *Diagram associating bone, cartilage, or fibrous tissue differentiation on function of inlet parameters determined by the scaffold, SS and FSS [11].*

For the simulations performed in this work different cell differentiation analysis were done (Fig. 13). Firstly, the SS obtained from the CSM model (for the static and dynamic cases) was evaluated to extract the element ratio differentiation only considering the X-axis classification. The same was done for the FSS resulting from the CFD model (with both fluid profiles) but only contemplating the Y-axis. Secondly, in order to acquire the cell differentiation distribution bearing in mind both parameters, a node coupling of both nodes was performed to determine the common nodes, then the stimuli S was calculated for every node. Thirdly, the FSS obtained with the FSI models that did not include displacements, was analysed only by contemplating the Y-axis. Then these results were compared to the CFD results but only taking into account the sharing nodes (as the interaction surface of the FSI did not entail the inferior surface of the scaffold). Finally, for the FSI models with deformation, a coupling of FSS and SS results was done and then compared with the ones obtained using CSM and CFD.

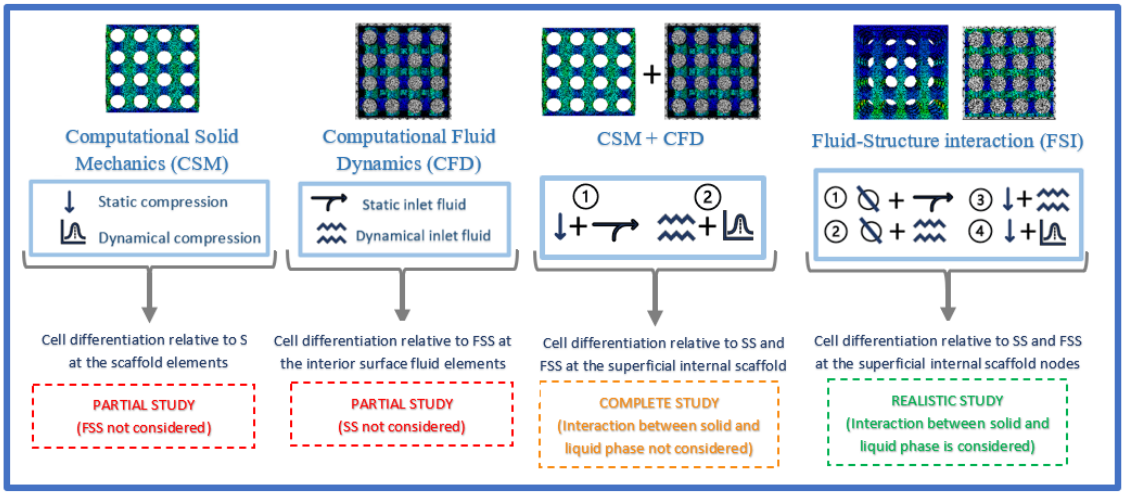

Figure 13. *Diagram explaining the different computational approaches used in the study to determine the bone differentiation of the different scaffold conformations. (1) CSM was considered a partial study since SS results are considered but the fluid phase stimulation is excluded. (2) CFD was considered a partial study since FSS results are considered but the solid phase stimulation is excluded. (3) The correlation between the CSM and CFD results is considered a more complete study than the others previous mentioned as the solid and the fluid phase are considered but is not realistic since there is no real interaction between the fluid and the scaffold surfaces. (4) The most realistic study done in this thesis is the FSI model in which the solid and fluid phases are considered and there is interaction between the surfaces.*

4. Results

4.1. Mechanical properties of the scaffolds

As it can be seen in Table 5, with higher porosities the E_f decreases and with lower increases. Being the maximum E_f obtained with C_60 and the minimum S_80. Moreover, the cylinder pore-based scaffolds present higher E_f values than the sphere pore-based.

Table 5. *Effective Young's Modulus of each scaffold design computed with the results obtained from CSM at static compression and implementing Equation 1.*

Effective Young's Modulus (GPa)					
C_60	**S_60**	**C_70**	**S_70**	**C_80**	**S_80**
0.992	0.684	0.771	0.582	0.625	0.516

From Figure 14 it can be observed that the percentage of elements in compression are notably higher than the tension ones, and the differences between porosities are minimal (for porosity 70% see Fig. SI-29). At 60% of porosity the maximum elements on compression are achieved for both conformation types, presenting the C_60 87.8% elements in compression and S_60 89.3% (Fig 13.A). The lower values are achieved at 80% porosity with 77.2% and 84% of elements in compression for C_80 and S_80 respectively (Fig 14.B). Furthermore, Figure 15 shows the stress distribution on cylinder and spherical scaffolds after the CSM was done and can be observed that the majority of compression and tension stress are located in the horizontal areas between the pores.

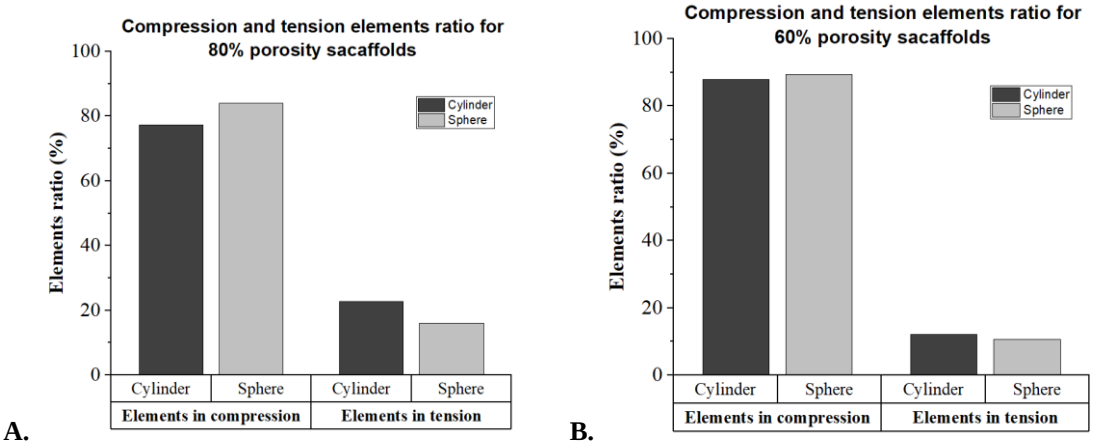

Figure 14. *Elements classification depending on the type of stress subjected: (a) Compression and tension elements ratio for 60% porosity and (b) Compression and tension elements ratio for 80% porosity.*

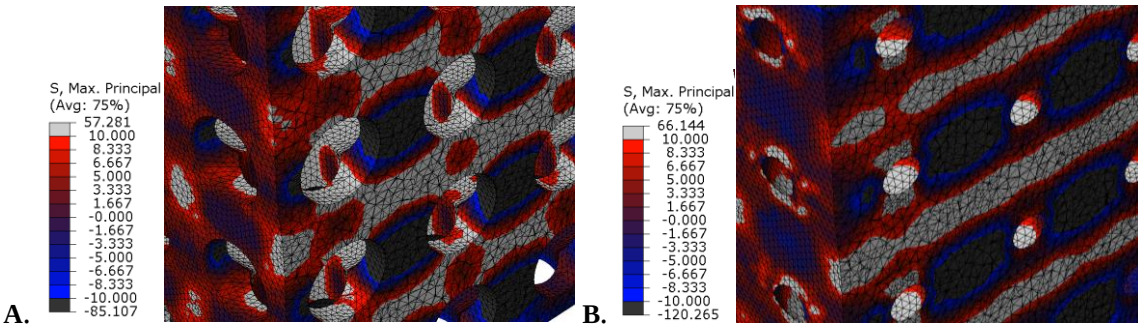

Figure 15. *View of the 60% porosity scaffolds showing the absolute Stress and Strain scale, highlighting the compression areas in blue and black and the tension areas in red: (a) C_60 scaffold, (b) S_60 scaffold.*

4.2. Cell differentiation study using Computational Solid Mechanic models

After analysing the SS values obtained from the CSM models, in which only the solid phase is considered, a phenotype distribution can be extracted. Firstly, the results applying steady deformation equal to 5% (Fig. 16) indicate relative high bone differentiation values for most of the conformations (for porosity 70% see Fig. SI-30), being C_80 the maximum value with 76% and S_60 the lowest with 51.4% bone. If the scaffolds are compared, cylinder scaffolds present a bone differentiation increment with respect to the spherical ones. In addition, low porosity presents less bone phenotype than high porous one.

Secondly, observing the cell differentiation values at dynamic compression (Fig. 17) similar results can be extracted than with static stimulation. The distance between bone tissue and cartilage differentiation percentage is wider for cylinder scaffolds and at high porosity. At low deformation (first time period and last time period) the bone phenotype is clearly predominantly, with low differentiation of cartilage and fibrous tissue. However, when the compression stimuli increase (middle time period) bone tissue decreases and the other two (more rapidly cartilage) increase.

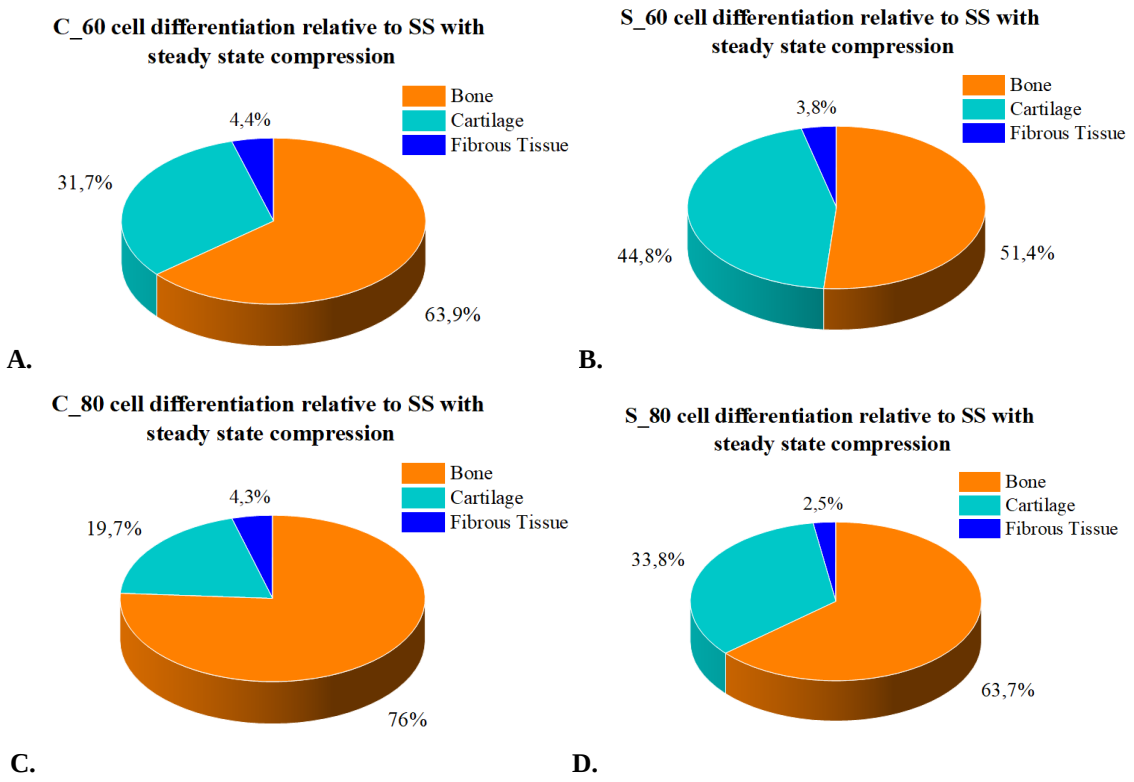

Figure 16. *Cell differentiation relative to SS results in the superficial nodes using CSM at steady state compression, being bone differentiation orange, cartilage differentiation cartílage light blue and fribrous tissue differentiaion dark blue.(a) C_60, (b) S_60, (c) C_80 and (d) S_80.*

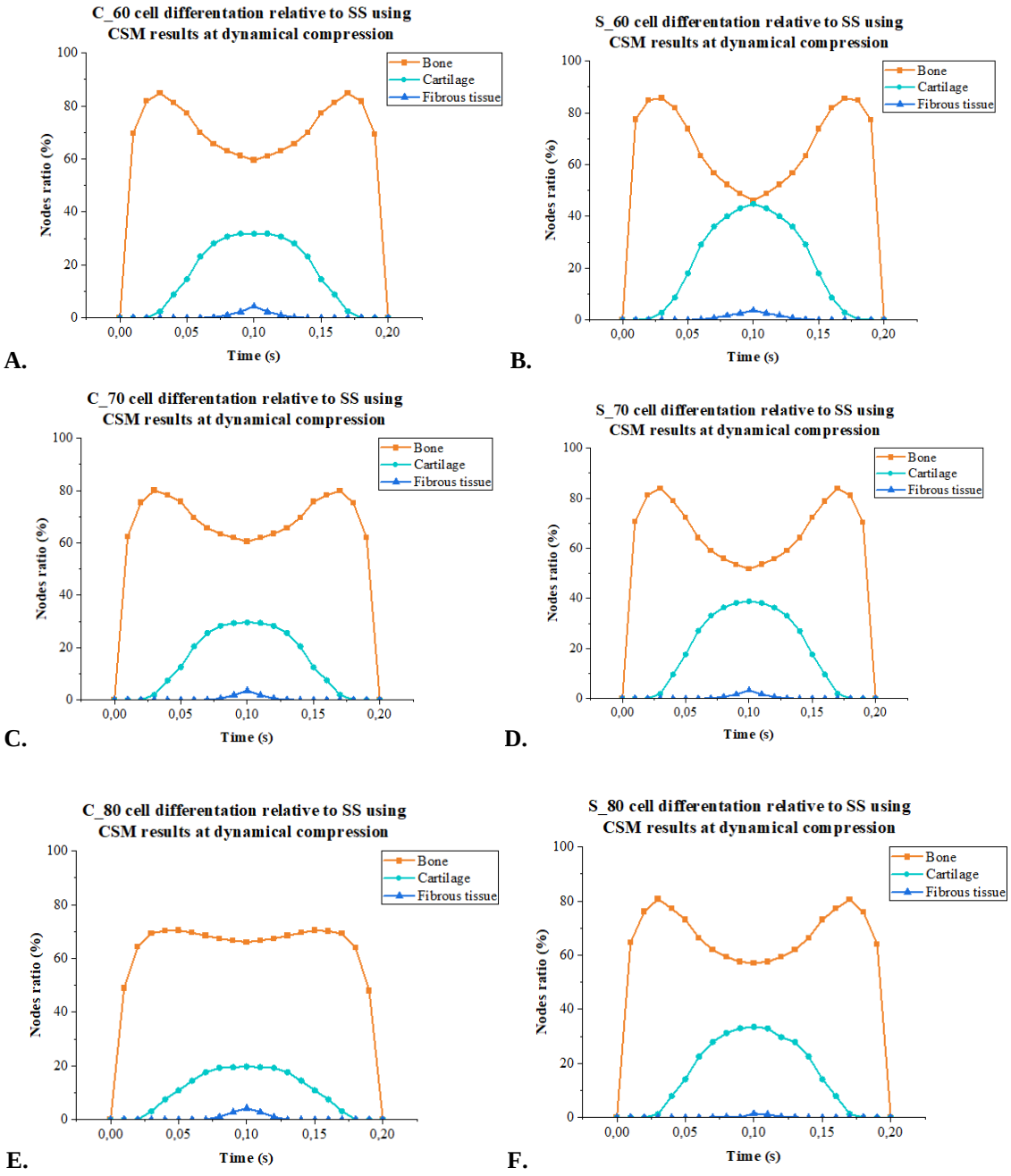

Figure 17. *Cell differentiation relative to SS results in the superficial nodes using CSM at dynamic compression, being bone differentiation orange, cartilage differentiation cartílage light blue and fribrous tissue differentiaion dark blue. (a) C_60, (b) S_60, (c) C_70 and (d) S_70, (e) C_80 and (f) S_60.*

4.3. Cell differentiation study using Computational Fluid Transient state models

The results obtained from CFD at transient state fluid profile that can be observed in Figure 18 show extremely low values of bone tissue differentiation (for porosity 70% see Fig. SI-31). The differences between scaffolds are significantly small with a certain increment in the bone differentiation at low porosities. Contrarily, the percentage of fibrous tissue differentiation is remarkably high in comparison with bone.

At transient state stimulation the graphs belonging to Figure 19 show a peak of bone differentiation at slow velocity (first time period and last time period), followed by another peak of cartilage differentiation and a delayed and wider peak of fibrous tissue differentiation. Connecting these graphs with the velocities presented in Figure 20, it can be seen that lower velocities are linked with higher bone differentiation peaks, achieving the maximum peak for C_80 with 52.46% and S_80 with 44.57%. Moreover, in figure 20 it can be observed certain fluid flows that collide and impact in the wall scaffold.

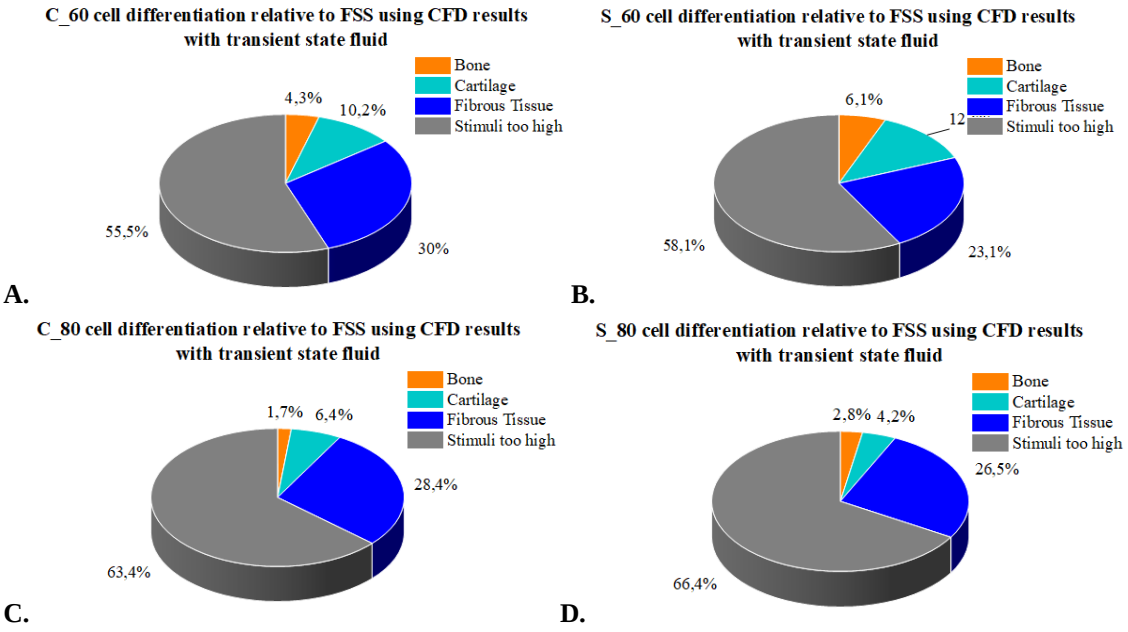

Figure 18. *Cell differentiation relative to FSS results in the superficial nodes using CFD at steady state inlet fluid, being bone differentiation orange, cartilage differentiation cartílage light blue, fribrous tissue differentiaion dark blue and stimuli too high to promote tissue differentiation .(a) C_60, (b) S_60, (c) C_80 and (d) S_80.*

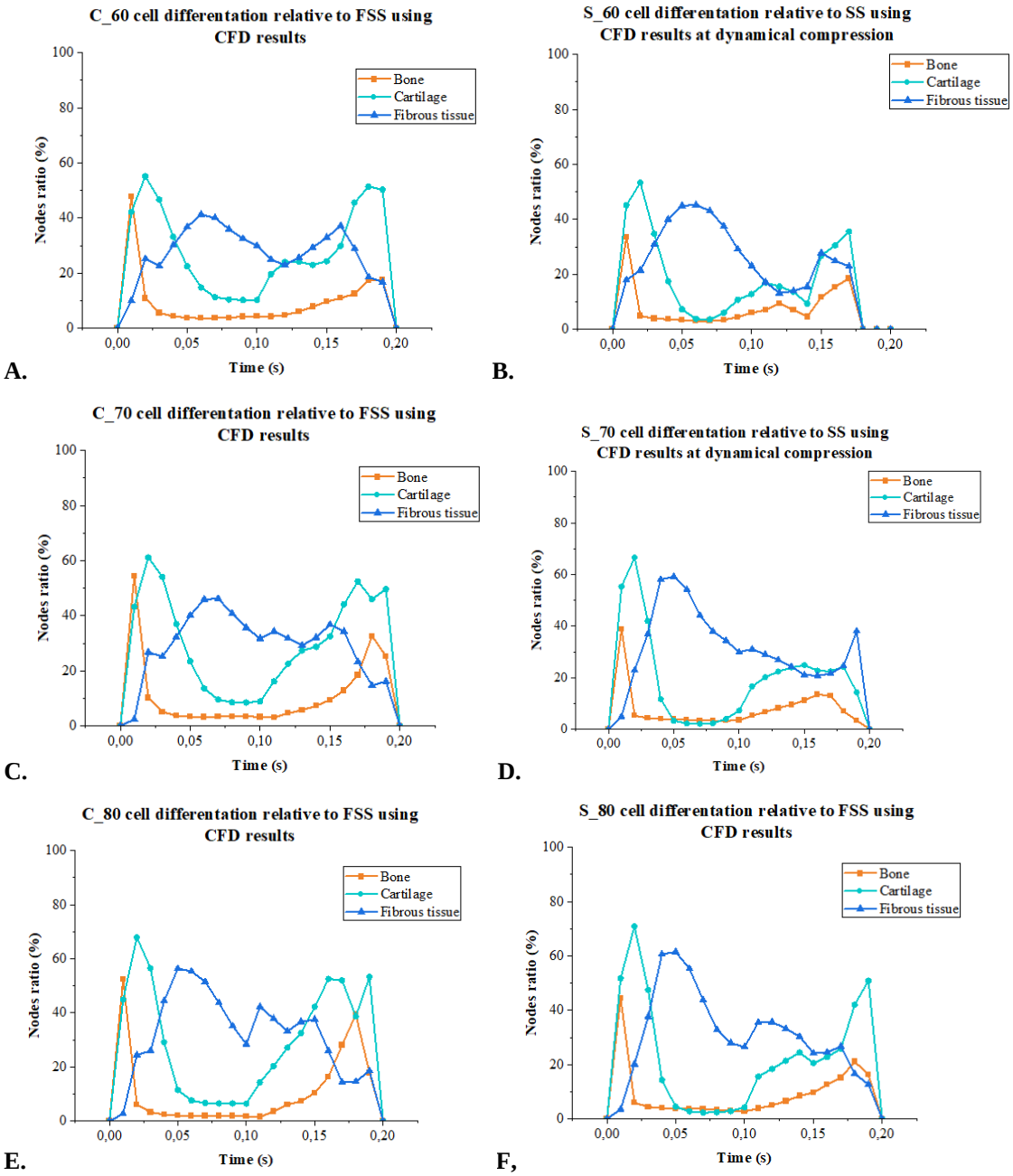

Figure 19. *Cell differentiation relative to SS results in the superficial nodes using CFD at transient state fluid profile, being bone differentiation orange, cartilage differentiation cartílage light blue and fribrous tissue differentiaion dark blue. (a) C_60, (b) S_60, (c) C_70 and (d) S_70, (e) C_80 and (f) S_60.*

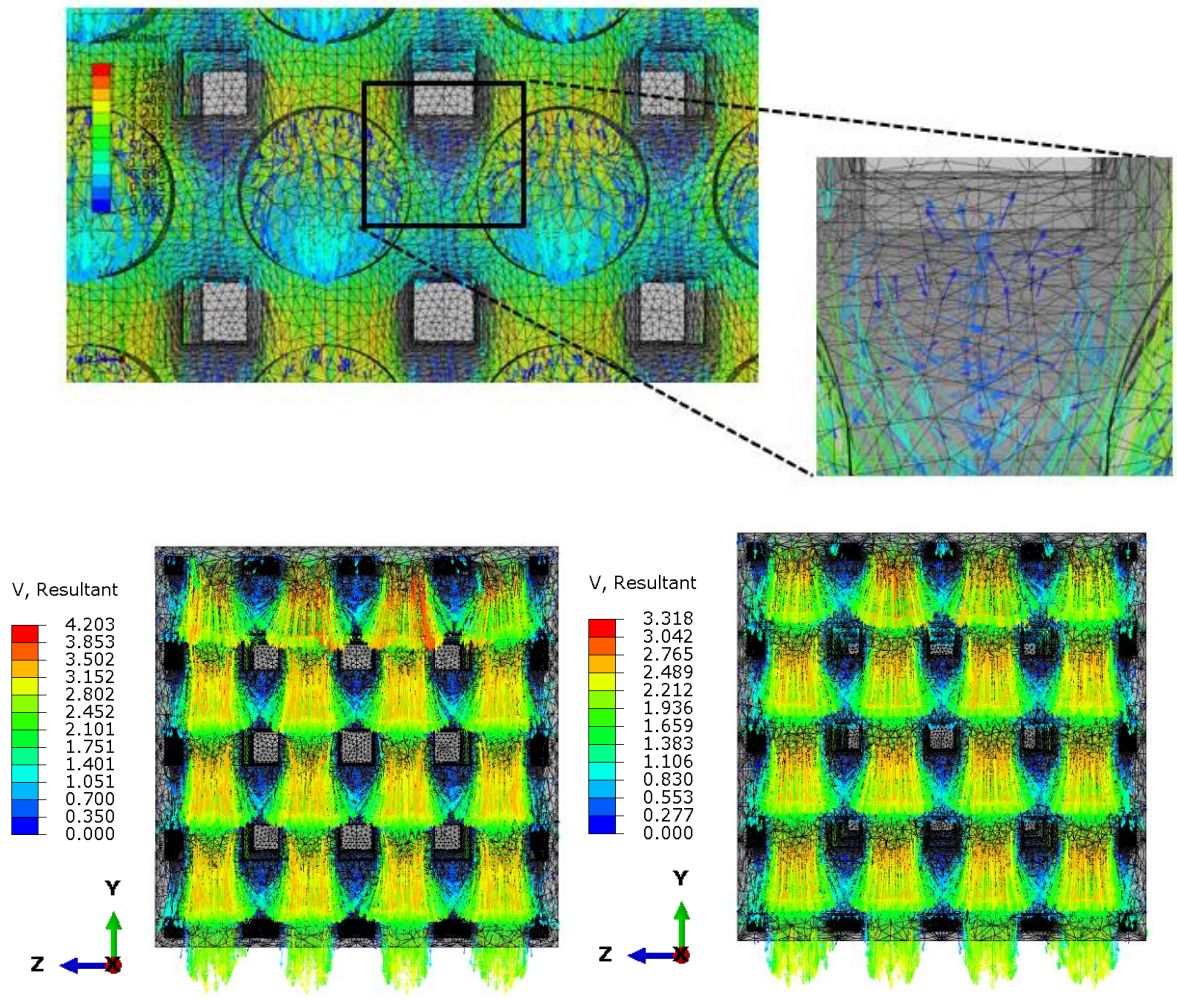

Figure 20. *CFD velocity vector colour map results at maximum fluid perfusion equal to 1 mm/s (top) fluid flows that collide and then impact in the wall scaffold in C_70, (left) velocity results for C_60, and (right) velocity results for C_70.*

4.4. Cell differentiation study using Computational Solid Mechanics and Computational Fluid Transient states

Using the SS results obtained from CSM models and FSS values obtained from CFD models, the S stimuli has been computed for the superficial nodes. The results obtained and presented in Figure 21 showed no differentiation in bone tissue for all the scaffolds in most of the time (please notice that Y-axis is rescaled). However, some extremely low peaks appeared at S_80 and C_80 at low fluid and mechanical stimulation. Furthermore, in Figure 22 it can be observed that the majority of the stimulation obtained is too high to promote tissue formation.

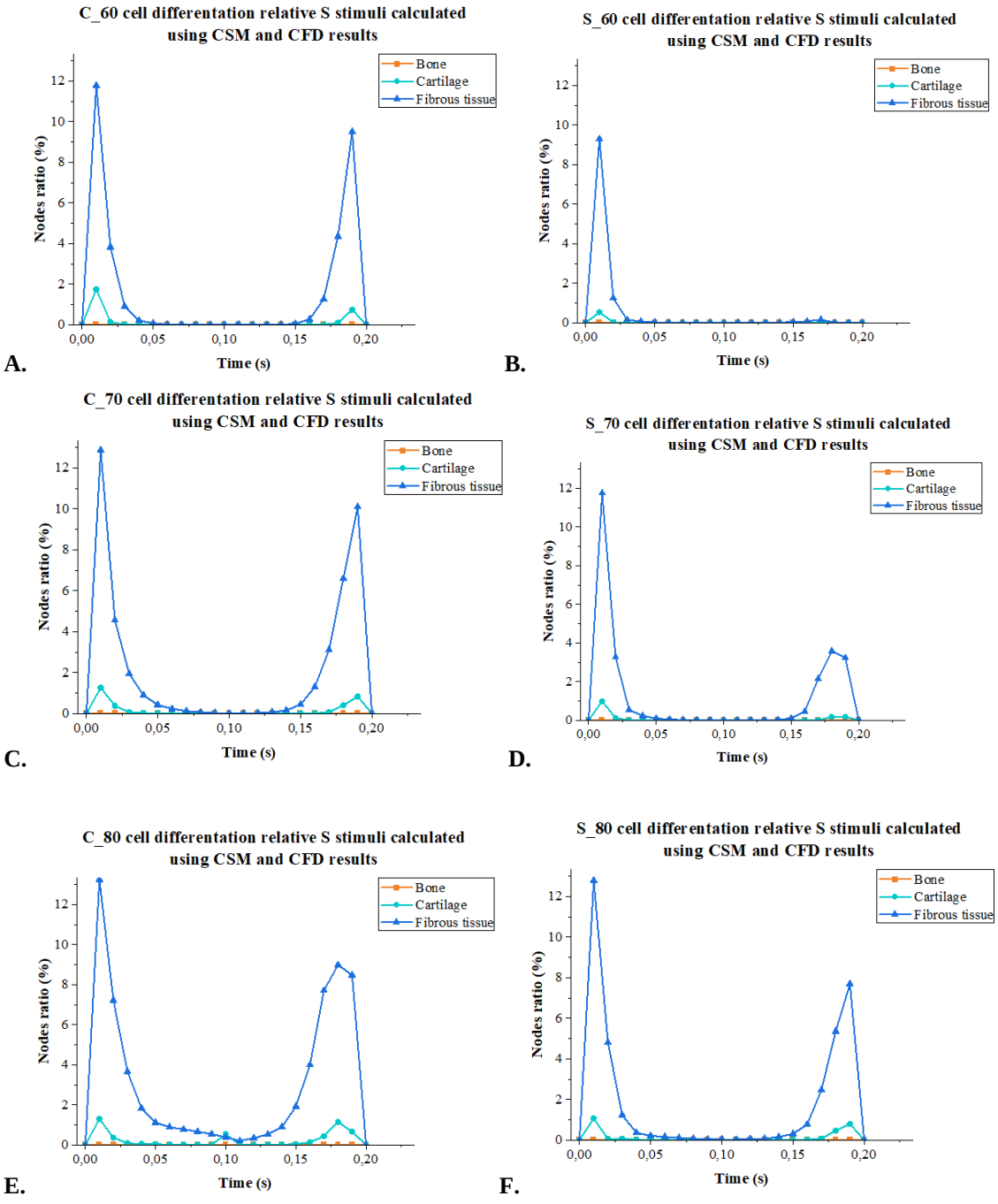

Figure 21. *Cell differentiation relative to S stimuli calculated with Equation 3, using the FSS results obtained with CFD models at transient state fluid perfusion and SS results obtained with CSM models at dynamic compression. Rescaled axis and presenting bone differentiation orange, cartilage differentiation cartílage light blue and fibrous tissue differentiation dark blue. (a) C_60, (b) S_60, (c) C_70 and (d) S_70, (e) C_80 and (f) C_80.*

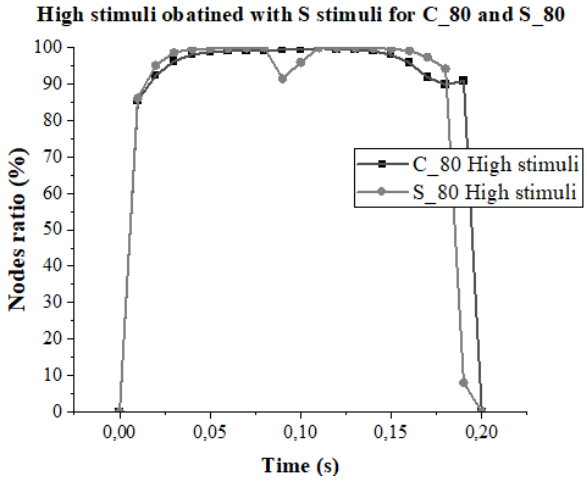

Figure 22. *High stimuli obtained after calculating S stimuli using FSS obtained performing CFD and SS obtained performing CSM simulation. C_80 scaffold is presented in Black and S_80 scaffold in grey.*

4.5. Cell differentiation study using Fluid-Structure Interaction models

Finally, fluid-structure interaction models were implemented with different stimulation conditions. Figure 23 shows the cell differentiation of FSI models in which transient state fluid profile was implemented and no compression was done. It can be observed that bone tissue differentiation results at a maximum velocity, equal to 1 mm/s, are extremely low. Moreover, Figure 24 showed differences between the results obtained using CFD results and FSI results, as the first peak is inferior to the one presented in the CFD results, and the second peak is quite decreased. The model presenting higher differences is C_80 in which it can be seen that its second peak is almost suppressed. Contrarily, S_80 is the scaffold conformation that obtained the higher second peak, even so it is highly decreased. Besides, Figure 25 shows the deformation caused by the fluid in the scaffold.

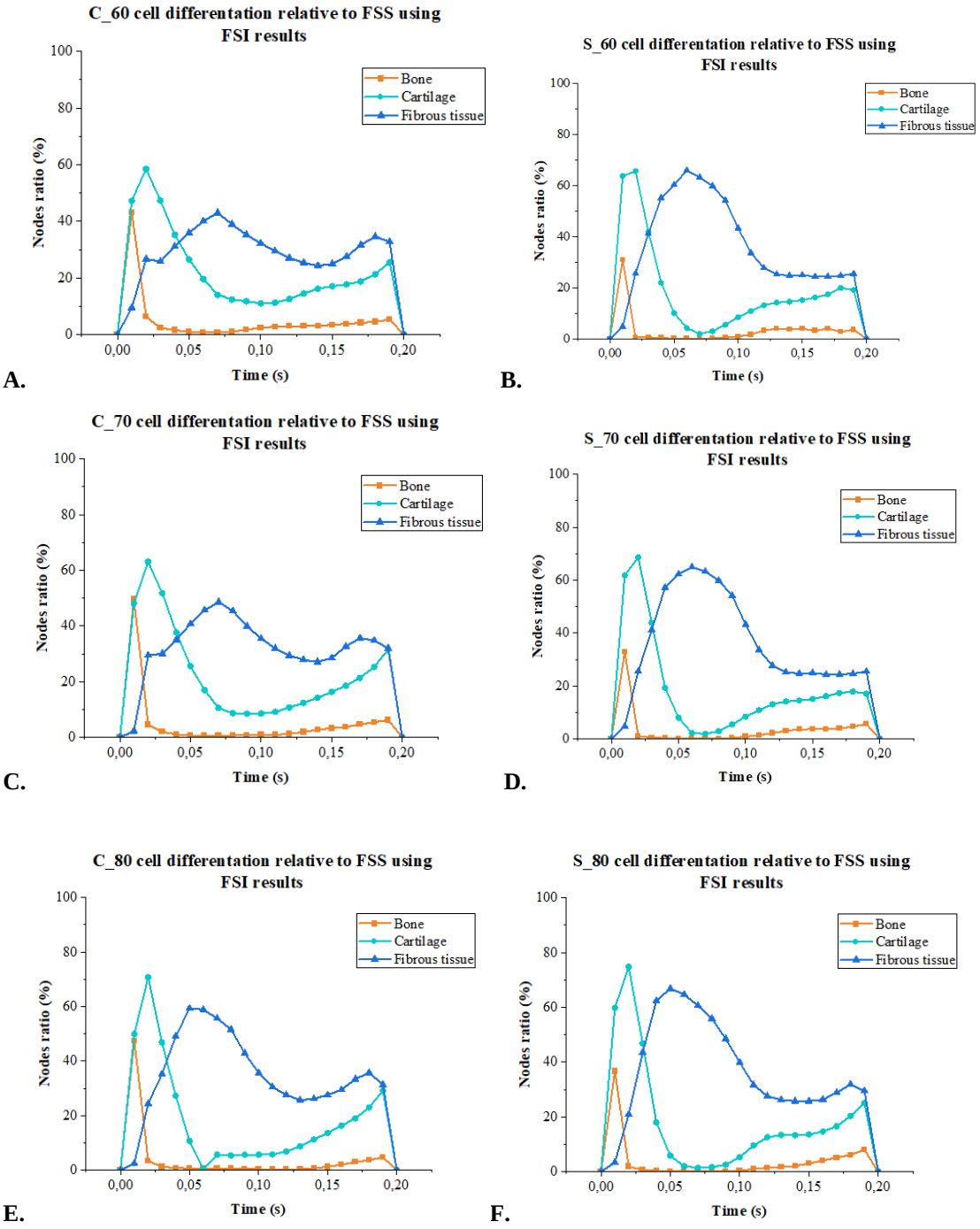

Figure 23. *Cell differentiation relative to FSS results in the superficial nodes using FSI at dynamic transient state fluid profile with no compression, being bone differentiation orange, cartilage differentiation cartílage light blue and fibrous tissue differentiation dark blue. (a) C_60, (b) S_60, (c) C_70 and (d) S_70, (e) C_80 and (f) C_80.*

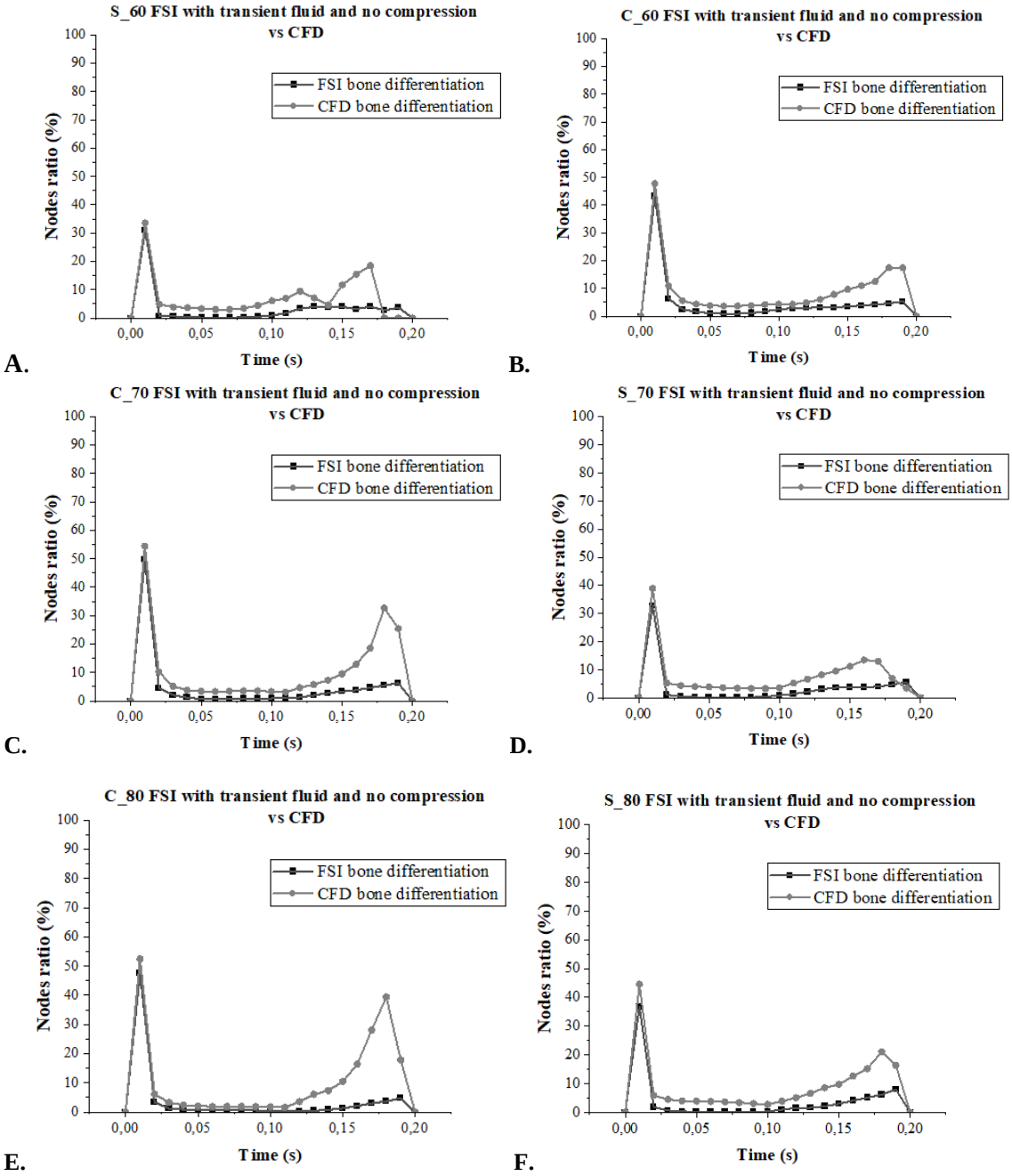

Figure 24. *Bone differentiation comparison between FSS results obtained using FSI model with transient state fluid and no compression (black), and FSS results obtained using CFD models (grey). (a) C_60, (b) S_60, (c) C_70 and (d) S_70, (e) C_80 and (f) C_80.*

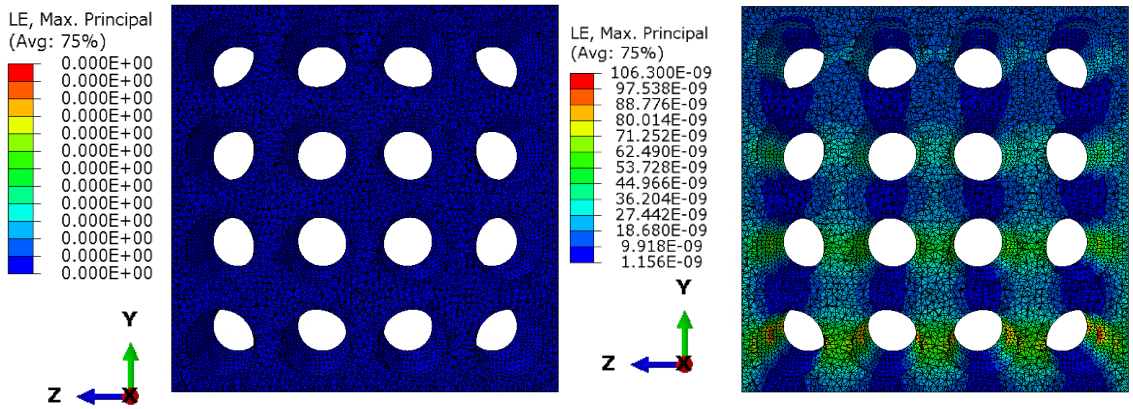

Figure 25. *SS colour map of the S_80 scaffold caused by the fluid stimuli: (left) before the fluid was perfused and () after the fluid was perfused.*

The results obtained from FSI models steady state compression and fluid flow for the S_80 scaffold show no differentiation of any type of tissue (Fig. 26.A). And the same is stated when the simulation is performed at steady compression and transient state fluid (Fig. 26.B). Accordingly, it is shown that the S stimuli is too high to promote any tissue differentiation as it was obtained in section 4.4. Moreover, in Figure 27 are shown the SS results after a sustained velocity of 1 mm/s and 5% deformation.

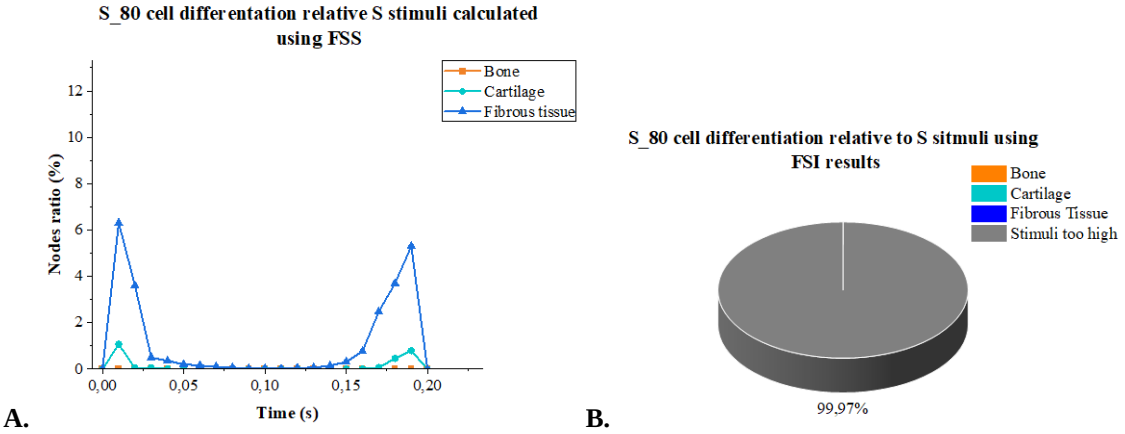

Figure 26. *Results obtained implementing a FSI model with S_80 scaffold. (a) steady state fluid and static compression and (b) with transient state fluid and dynamic compression.*

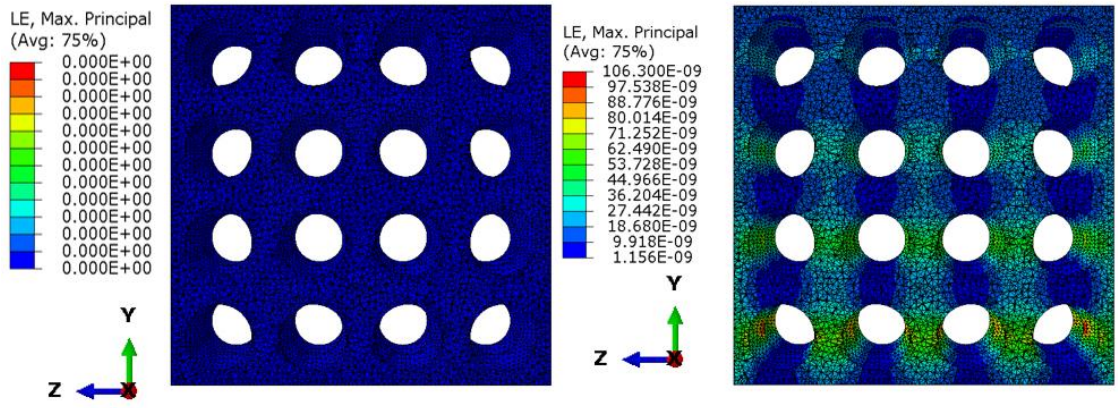

Figure 27. SS colour map of the S_80 scaffold caused by steady state fluid perfusion at 1 mm/s and static compression of 5%: (a) before the simulation was done and (a) after the simulation was implemented.

5. Discussion

The fundamental objective of the thesis was to conduct a fluid-structure analysis on different scaffold conformations to find the optimal configuration that led to bone cell differentiation enough to repair a fracture. For the cell differentiation evaluation, different computational techniques were employed.

On the one hand, CSM models demonstrated that all the scaffold geometries designed in this thesis showed enough mechanical properties to be considered as a possible bone substitute. As it can be observed in Table 5, all the Ef values obtained are similar to Young's Modulus established for the scaffold material. As it is known, PDLLA is a material that has already been widely applied in BTE because of its suitable mechanical properties, so the scaffolds presented seem to maintain resemblant characteristics [26]. Moreover, from Figure 14, it can be extracted that most elements in all the conformations are at compression stress, which is positive as it is generally accepted that bone strength is greater in compression than in tension [42].

On the other hand, centring the attention on the cell differentiation study relative to SS using CSM, it can be concluded that these models were helpful as they confirmed that compressions between a range of 0 to 5% are crucial to obtaining high percentages of bone phenotype. However, the studies also indicate that maximum compressions were less favourable for bone tissue differentiation (see Fig. 16). For instance, the S_60 scaffold presented a similar differentiation percentage for bone and cartilage at high deformations (51.4% and 44.8%, respectively), increasing the risk of mechanical failure. It is essential to highlight that cartilage and fibrous tissue do not possess the same mechanical properties as bone; hence the presence of significant regions of these tissues can cause instability and even another fracture. Therefore, it could be stated that cylinder pore-based scaffolds with high porosity could be more optimal than the sphere-based. Since cylinder scaffolds achieved lower cartilage and fibrous tissue differentiation, the bone values remained more stable in comparison with the sphere scaffolds during the transient state deformation. This observation can suggest that cylinder scaffolds are transmitting lower SS stimuli than sphere pore based but high enough to remain within the range needed for bone tissue differentiation. Consequently, since stimulus cannot be controlled in a natural environment, contrary to a bioreactor, it could be more positive to have a scaffold presenting lower and more stable peaks of bone differentiation and lower phenotype presence of other tissue types.

Focusing on the cell differentiation results obtained relative to FSS using CFD, it can be concluded that relevant bone differentiation can be achieved only with low velocities. At very low velocities, a peak of bone phenotype was found, rapidly followed by a peak of cartilage. In addition, it can be observed that an increment of the velocity entailed a notable presence of fibrous tissue differentiation, while bone and cartilage were drastically decreased. For this reason, it can be concluded using CFD models that 1 mm/s is too high to obtain satisfactory rates of bone tissue differentiation. Nonetheless, this is not negative as the irrigation known in the canaliculi channels is around the μm/s magnitude, so in theory, this could not represent a problem in a clinical application [43]. Even so, if only the fluid stimulation is considered, it seems complicated to obtain enough bone differentiation and avoid regions with another tissue type. Since at low velocities, the cartilage tissue is remarkably present using these scaffold designs even at high porosity conformations that seem to obtain the best results.

Furthermore, velocity and bone phenotype can be correlated (see Fig. 19 and 20), as high bone differentiation peaks are achieved when the velocity rate is low. A clear example of this is the comparison between the high porous scaffold and low ones; the first type presents lower velocities than the second one (Fig. 20), and accordingly, the ranges of bone differentiation are higher for high porous scaffolds than for low porous scaffolds. However, it is essential to clarify that scaffolds with lower porosities often achieved better bone phenotype results than high porous ones. However, since these fluid perfusion rates have been confirmed too high to obtain sufficient bone differentiation (percentages are too low), this does not affect the conclusion. Moreover, this clarification agrees with the results of Ouyang et al. and Fu et al., since if pore size increases, FSS will also augment. For this reason, when the fluid perfusion velocity achieves high rates, the FSS values will increase more in high porous scaffolds than in lower ones. Therefore, as Figure 11 indicates, high FSS values do not promote bone tissue differentiation.

Nevertheless, a coupling between the mechanical and fluid results was made to obtain a more realistic analysis of the stimulation that mesenchymal stem cells could undergo. The results shown in Figure 21 reiterate the conclusions extracted in the previous models. Only some bone cell differentiation is present when the fluid flow is minimum, and the compression is low due to an excessive high stimulation that inhibits cell differentiation (see Fig. 22). Additionally, it is reaffirmed that high porous scaffolds present better results than low porous, which can be results obtained for the SS study. Considering that high porosity scaffolds achieved better results in mechanical stimulation than with fluid simulation, it is possible to conclude that compression deformation will be fundamental to obtaining bone differentiation at low velocities and inhibiting cartilage differentiation. Besides, if sphere and cylinder conformations are compared, cylinder pore-base achieves better results; hence neither of them with the velocities considered in this study could obtain significant results to restore a bone fracture. Despite these results, it could be interesting to analyse these scaffolds with the same deformation range at low velocities to be capable of discerning the actual application of these scaffold designs.

Most studies until now have evaluated the scaffold performance and predicted its adequate application in BTE, contemplating the solid and liquid phases as independent parts [14,15]. Accordingly, even though they present an FSI study, there is no real interaction between the two parts in this simulation. What is commonly done is to perform a CFD simulation, assuming that due to the high Young Modulus scaffold, there cannot exist any deformation of the scaffold caused by the fluid [14]. Then, the pressure results obtained from the CFD are introduced to a CSM model, and the compression is done. So, knowing this strategy, a critical objective of the study was to verify if performing a model in which the scaffold and the fluid were able to interact, the results remained the same or were insignificant. Nonetheless, as it is shown in Figure 24, it is clear that the results obtained were quite different.

The significant difference between a CFD and FSI model is that the first does not contemplate any interaction between the fluid and the scaffold wall, as the wall has no properties and has a 0-velocity. On the contrary, the FSI model, in this case without compression to make possible the comparison with CFD, allows the interaction between the fluid and the solid, conferring specific properties to the scaffold walls and not applying a 0-velocity requirement. As can be seen in Figure 24, even though, in the beginning, CFD and FSI seem to have similar behaviour, when the time increments, it can be seen

that the differences are increasing. This increase can be explained by the fact that the scaffold wall was defined as no-slip in the CFD cases, which means that the wall has zero velocity. Contrarily, the FSI model allows the deformation of the scaffold due to the fluid interaction (see Fig. 25) and the own properties of PDLLA; therefore, when the fluid impacts the wall, the velocity of the fluid will change, adopting the velocity of the wall during the deformation. These changes are translated into a smaller bone differentiation percentage that will be more affected depending on the scaffold deformation. Therefore, it could be stated that the studies in which only CFD models are applied can obtain an overestimation of their bone tissue differentiation. For this reason, FSI models that allow the interaction of the fluid and the scaffold are necessary for evaluating the scaffold designs for the BTE application.

Finally, the scaffold S-80 was chosen as it was the conformation with better results in the last part of the FSI study done with no compression and transient state fluid. Due to this, it was thought that this design could suffer minor deformation due to the fluid, so it could be interesting to see the results of adding an external compression. However, as mentioned before, the stimulation was too high to promote tissue differentiation. Therefore, it could not be possible to compare the results with those obtained correlating the CSM and CFD results since the differences could not be appreciated.

After performing all the simulations, it can be verified that the horizontal areas between the pores are where the stimuli are more present (Fig. 15, 25 and 27). In addition, in Figure 20, it can be observed specific fluid flows that collide and impact the wall scaffold. This observation could entail cell seeding in this area, indicating that cells could be attached in these zones where more mechanical and fluid stimulus has been found. So, this is a decisive observation since there is more certainty that external stimulation will affect mesenchymal cells.

Some limitations should be considered in this study. One of them is the computational cost of this type of simulation, since especially when an interaction between different parts must be considered, the computational time may increase up to 10 hours to finalise. However, it is essential to highlight that CSM and CFD models are faster than FSI, but as was concluded during the thesis, the results are not analogous between models. Moreover, the FSI models were performed without evaluating the top and bottom scaffold parts since some boundary conditions had to be applied to obtain a functional simulation. However, maybe the most limiting part of this study is the possible variability in the bone mechanical properties and the external environment depending on the patient. Since a bone of an 11-year-old child will not follow the same behaviour as a 60-adult woman.

6. Conclusions

In conclusion, the presented cell differentiation study stated that high porous scaffolds with low compression and fluid perfusion rates promote bone tissue phenotype. In addition, it was verified that the horizontal areas between porous present the most significant stimulation influence and cell attachment.

Moreover, it was demonstrated that studies in which interaction between the scaffold and fluid flow is not considered could lead to substantial overestimations of bone differentiation, as fluid can cause deformations in the scaffold, which reduces bone tissue formation. More specifically, the differences augment in dynamical environments closest to the clinical application.

During all the studies, it has been established the importance of SS stimulation for bone tissue differentiation together with FSS. Mechanical stimulation has been found to stimulate bone differentiation and inhibit cartilage phenotype.

Accordingly, to achieve a correct approximation to elucidate if a scaffold is optimal for successful bone fracture healing, a study mimicking the closest possible to the natural environment is needed. Therefore, the scaffold performance must be evaluated with dynamic mechanical and transient state fluid profile stimulation, and the interaction between the solid and fluid phases must be considered.

7. Future work

In future work, It could be interesting to prove the identical scaffold conformations with a lower velocity range. With this, more significant bone differentiation percentages can be obtained, and the results after computing S stimuli can be compared with FSI models. Moreover, the FSI study could also be extended to all the scaffold designs to complete the study. Finally, it could be interesting to implement the same methodology pipeline with a porous gradient scaffold, studying if there is any existent differentiation pattern. Moreover, it can also be verified if an evaluation not using the interaction between the solid and liquid phases could also lead to an overestimation of bone differentiation using these scaffold designs.

References

[1] Wu, A., Bisignano, C., James, S., Abady, G., Abedi, A., & Abu-Gharbieh, E. et al. (2021). Global, regional, and national burden of bone fractures in 204 countries and territories, 1990–2019: a systematic analysis from the Global Burden of Disease Study 2019. *The Lancet Healthy Longevity*, *2*(9), e580-e592. doi: 10.1016/s2666-7568(21)00172-0

[2] Fractures (Broken Bones) - OrthoInfo - AAOS. (2022). Available from: https://orthoinfo.aaos.org/en/diseases--conditions/fractures-broken-bones/

[3] Office of the Surgeon General (US)(2004) Bone Health and Osteoporosis: A Report of the Surgeon General. Rockville (MD): Office of the Surgeon General (US); 4, The Frequency of Bone Disease. Available from: https://www.ncbi.nlm.nih.gov/books/NBK45515/

[4] Hernlund, E., Svedbom, A., Ivergård, M., Compston, J., Cooper, C., & Stenmark, J. et al. (2013). Osteoporosis in the European Union: medical management, epidemiology and economic burden. *Archives Of Osteoporosis*, *8*(1-2). doi: 10.1007/s11657-013-0136-1

[5] Schemitsch, E. (2017). Size Matters: Defining Critical in Bone Defect Size!. *Journal Of Orthopaedic Trauma*, *31*(5), S20-S22. doi: 10.1097/bot.0000000000000978

[6] Fu M., Wang F., Lin G. (2021) Design and research of bone repair scaffold based on two-way fluid-structure interaction. Computer Methods and Programs in Biomedicine. Volume 204. https://doi.org/10.1016/j.cmpb.2021.106055

[7] Howard, D., Buttery, L. D., Shakesheff, K. M., & Roberts, S. J. (2008). Tissue engineering: strategies, stem cells and scaffolds. Journal of anatomy, 213(1), 66–72. https://doi.org/10.1111/j.1469-7580.2008.00878.x

[8] Adachi, T., Osako, Y., Tanaka, M., Hojo, M., & Hollister, S. (2006). Framework for optimal design of porous scaffold microstructure by computational simulation of bone regeneration. Biomaterials, 27 (21), 3964-3972. https://doi.org/10.1016/j.biomaterials.2006.02.039

[9] Amini, A., Laurencin, C., & Nukavarapu, S. (2012). Bone Tissue Engineering: Recent Advances and Challenges. *Critical Reviews™ In Biomedical Engineering*, *40*(5), 363-408. doi: 10.1615/critrevbiomedeng.v40.i5.10

[10] Sun, Y., Wan, B., Wang, R., Zhang, B., Luo, P., & Wang, D. et al. (2022). Mechanical Stimulation on Mesenchymal Stem Cells and Surrounding Microenvironments in Bone Regeneration: Regulations and Applications. *Frontiers In Cell And Developmental Biology*, *10*. doi: 10.3389/fcell.2022.808303

[11] Olivares, A., Marsal, È., Planell, J., & Lacroix, D. (2009). Finite element study of scaffold architecture design and culture conditions for tissue engineering. *Biomaterials*, *30*(30), 6142-6149. doi: 10.1016/j.biomaterials.2009.07.041

[12] Ouyang, P., Dong, H., He, X., Cai, X., Wang, Y., & Li, J. et al. (2019). Hydromechanical mechanism behind the effect of pore size of porous titanium scaffolds on osteoblast response and bone ingrowth. *Materials &Amp; Design*, *183*, 108151. doi: 10.1016/j.matdes.2019.108151

[13] Ali, D., & Sen, S. (2018). Computational Fluid Dynamics Study of the Effects of Surface Roughness on Permeability and Fluid Flow-Induced Wall Shear Stress in Scaffolds. *Annals Of Biomedical Engineering*, *46*(12), 2023-2035. doi: 10.1007/s10439-018-2101-z

[14] Zhao, F., Vaughan, T., & McNamara, L. (2015). Quantification of fluid shear stress in bone tissue engineering scaffolds with spherical and cubical pore architectures. *Biomechanics And Modeling In Mechanobiology*, *15*(3), 561-577. doi: 10.1007/s10237-015-0710-0

[15] Fu, M., Wang, F., & Lin, G. (2021). Design and research of bone repair scaffold based on two-way fluid-structure interaction. *Computer Methods And Programs In Biomedicine*, *204*, 106055. doi: 10.1016/j.cmpb.2021.106055

[16] Compound Fracture: What Is It, Types, Symptoms & Treatment. (2022). Available from: https://my.clevelandclinic.org/health/diseases/21843-compound-fracture

[17] Sheen, J., & Garla, V. (2022). Fracture Healing Overview. Available from: https://www.ncbi.nlm.nih.gov/books/NBK551678/

[18] Fracture Healing - Basic Science - Orthobullets. (2022). Available from: https://www.orthobullets.com/basic-science/9009/fracture-healing

[19] Strelzow, J., & Grewal, R. (2018). Predicting Union of Scaphoid Fractures. *Scaphoid Fractures: Evidence-Based Management*, 199-208. doi: 10.1016/b978-0-323-48564-7.00022-8

[20] Buckley, R., Page, J.L., (2021). General Principles of Fracture Care Treatment & Management. Medscape; Drugs & Disease; Orthopedic Surgery. Available from: https://emedicine.medscape.com/article/1270717-treatment

[21] Nunez, K. (2019) Repairing Major Bone Breaks with Open Reduction Internal Fixation Surgery. Healthline. Available from: https://www.healthline.com/health/orif-surgery

[22] Bone Grafting. Hopkinsmedicine.org. (2022). Available from: https://www.hopkinsmedicine.org/health/treatment-tests-and-therapies/bone-grafting.

[23] Hollister, S. (2005). Porous scaffold design for tissue engineering. Nature Materials, 4(7), 518-524. https://doi.org/10.1038/nmat1421

[24] Chan, B., & Leong, K. (2008). Scaffolding in tissue engineering: general approaches and tissue-specific considerations. *European Spine Journal*, *17*(S4), 467-479. doi: 10.1007/s00586-008-0745-3

[25] Velasco, M., Narváez-Tovar, C., & Garzón-Alvarado, D. (2015). Design, Materials, and Mechanobiology of Biodegradable Scaffolds for Bone Tissue Engineering. Biomed Research International, 2015, 1-21. https://doi.org/10.1155/2015/729076

[26] Shah Mohammadi, M., Rezabeigi, E., Bertram, J., Marelli, B., Gendron, R., Nazhat, S., & Bureau, M. (2020). Poly(d,l-Lactic acid) Composite Foams Containing Phosphate Glass Particles Produced via Solid-State Foaming Using CO2 for Bone Tissue Engineering Applications. Polymers, 12(1), 231. https://doi.org/10.3390/polym12010231

[27] Bose, S., Vahabzadeh, S., & Bandyopadhyay, A. (2013). Bone tissue engineering using 3D printing. Materials Today, 16(12), 496-504. https://doi.org/10.1016/j.mattod.2013.11.017

[28] Yousefi, A., James, P., Akbarzadeh, R., Subramanian, A., Flavin, C., & Oudadesse, H. (2016). Prospect of Stem Cells in Bone Tissue Engineering: A Review. Stem Cells International, 2016, 1-13. https://doi.org/10.1155/2016/6180487

[29] Oryan, A., Kamali, A., Moshiri, A., & Baghaban Eslaminejad, M. (2017). Role of Mesenchymal Stem Cells in Bone Regenerative Medicine: What Is the Evidence?. Cells Tissues Organs, 204(2), 59-83. https://doi.org/10.1159/000469704

[30] Carpentier, B., Layrolle, P., & Legallais, C. (2011). Bioreactors for Bone Tissue Engineering. The International Journal Of Artificial Organs, 34 (3), 259-270. https://doi.org/10.5301/ijao.2011.6333

[31] Yeatts, A., & Fisher, J. (2011). Bone tissue engineering bioreactors: Dynamic culture and the influence of shear stress. Bone, 48 (2), 171-181. https://doi.org/10.1016/j.bone.2010.09.138

[32] Rauh, J., Milan, F., Günther, K., & Stiehler, M. (2011). Bioreactor Systems for Bone Tissue Engineering. Tissue Engineering Part B: Reviews, 17 (4), 263-280. https://doi.org/10.1089/ten.teb.2010.0612

[33] ladkova, M., & de Peppo, G. (2014). Bioreactor Systems for Human Bone Tissue Engineering. Processes, 2 (2), 494-525. https://doi.org/10.3390/pr2020494

[34] Stanbury, P., Whitaker, A., & Hall, S. (2017). Design of a fermenter. Principles Of Fermentation Technology, 401-485. doi: 10.1016/b978-0-08-099953-1.00007-7

[35] Fu, M., Wang, F., & Lin, G. (2021). Design and research of bone repair scaffold based on two-way fluid-structure interaction. Computer Methods And Programs In Biomedicine, 204, 106055. doi: 10.1016/j.cmpb.2021.106055

[36] Lacroix, D., Prendergast, P., Li, G., & Marsh, D. (2002). Biomechanical model to simulate tissue differentiation and bone regeneration: Application to fracture healing. *Medical &Amp; Biological Engineering &Amp; Computing*, *40*(1), 14-21. doi: 10.1007/bf02347690

[37] Zeltinger, J., Sherwood, J., Graham, D., Müeller, R., & Griffith, L. (2001). Effect of Pore Size and Void Fraction on Cellular Adhesion, Proliferation, and Matrix Deposition. Tissue Engineering, 7(5), 557-572. doi: 10.1089/107632701753213183

[38] Dallas, S., Prideaux, M., & Bonewald, L. (2013). The Osteocyte: An Endocrine Cell … and More. Endocrine Reviews, 34(5), 658-690. doi: 10.1210/er.2012-1026

[39] Wang, Zhao, Fuh, & Lee. (2019). Effect of Porosity on Mechanical Properties of 3D Printed Polymers: Experiments and Micromechanical Modeling Based on X-Ray Computed Tomography Analysis. Polymers, 11(7), 1154. doi: 10.3390/polym11071154

[40] Casalini, T., Rossi, F., Castrovinci, A., & Perale, G. (2019). A Perspective on Polylactic Acid-Based Polymers Use for Nanoparticles Synthesis and Applications. Frontiers In Bioengineering And Biotechnology, 7. doi: 10.3389/fbioe.2019.00259

[41] Lacroix, D., & Prendergast, P. (2002). A mechano-regulation model for tissue differentiation during fracture healing: analysis of gap size and loading. *Journal Of Biomechanics*, *35*(9), 1163-1171. doi: 10.1016/s0021-9290(02)00086-6

[42] Morgan, E., Barnes, G., & Einhorn, T. (2013). The Bone Organ System. *Osteoporosis*, 3-20. doi: 10.1016/b978-0-12-415853-5.00001-7

[43] Gatti, V., Gelbs, M., Guerra, R., Gerber, M., & Fritton, S. (2021). Interstitial fluid velocity is decreased around cortical bone vascular pores and depends on osteocyte position in a rat model of disuse osteoporosis. *Biomechanics And Modeling In Mechanobiology*, *20*(3), 1135-1146. doi: 10.1007/s10237-021-01438-4

Supporting information

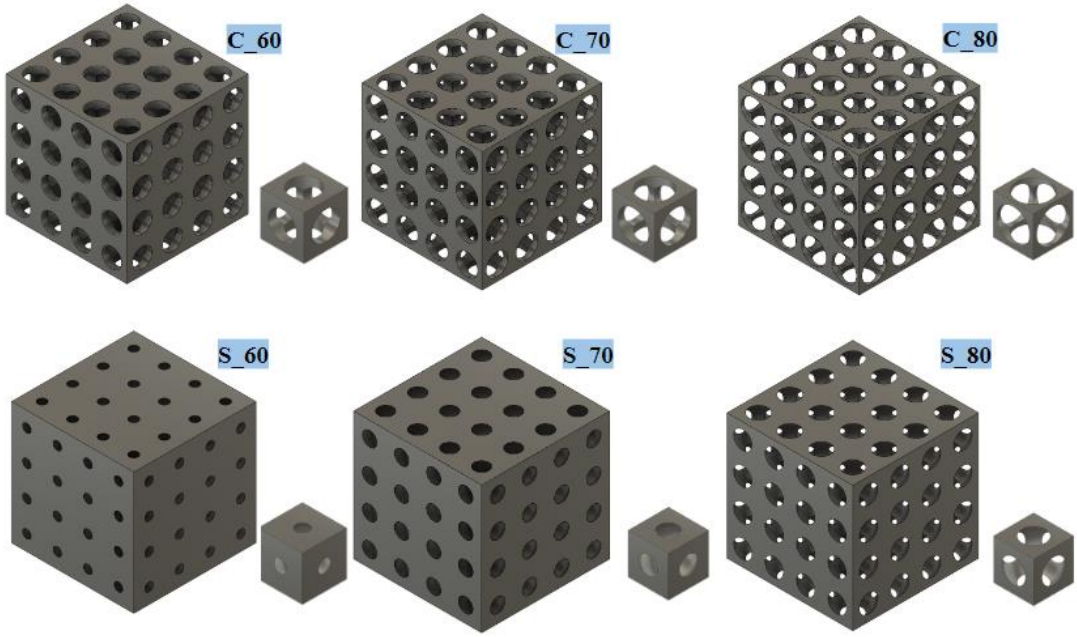

Figure SI-28. *Scaffolds are designed with three different porosity (60, 70 and 80%) and two geometrical pore configuration, cylindrical and spherical.*

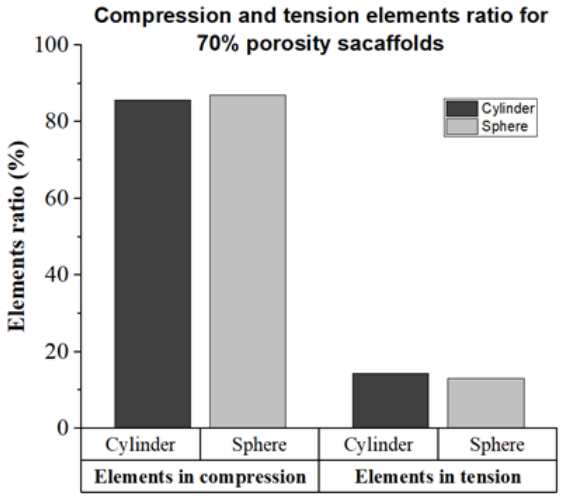

Figure SI-29. *Elements classification depending on the type of stress subjected; Compression and tension elements ratio for 70% porosity.*

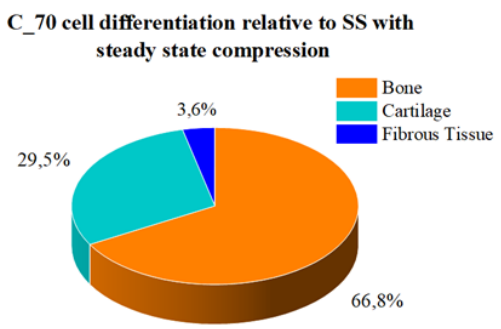

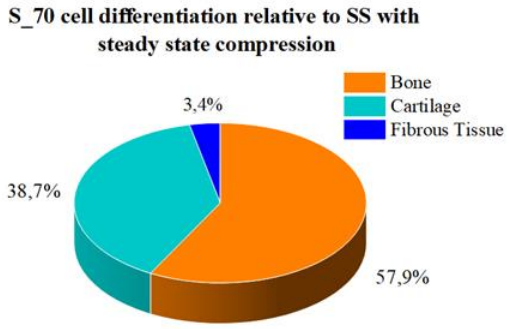

A. **B-**

Figure SI-30. *Cell differentiation relative to SS results in the superficial nodes using CSM at steady state compression, being bone differentiation orange, cartilage differentiation cartilage light blue and fibrous tissue differentiation dark blue. (a) C_70 and (b) S_70.*

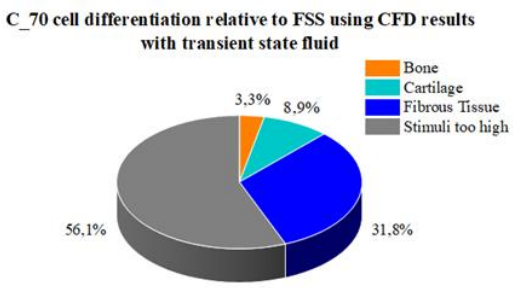

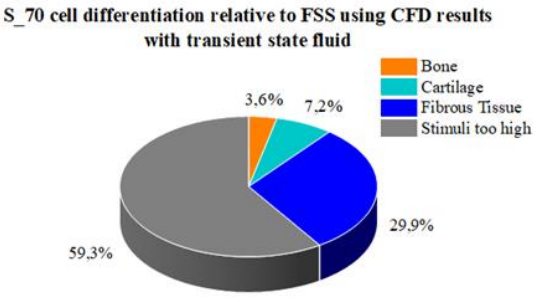

A. **B.**

Figure SI-31. *Cell differentiation relative to FSS results in the superficial nodes using CFD at steady state inlet fluid, being bone differentiation orange, cartilage differentiation cartílage light blue, fibrous tissue differentiation dark blue, and stimuli too high to promote tissue differentiation .(a) C_70 and (b)S_70.*